USING SELF-ORGANIZING MAPS TO UNDERSTAND THE EFFECTS OF SYNOPTIC CONFIGURATIONS ON WESTERN NORTH PACIFIC TROPICAL CYCLONES

BY

FANGYI ZHOU

THESIS

Submitted in partial fulfillment of the requirements
for the degree of Master of Science in Atmospheric Sciences
in the Graduate College of the
University of Illinois Urbana-Champaign, 2022

Urbana, Illinois

Master's Committee:

Professor Stephen Nesbitt, Adviser
Professor Zhuo Wang
Assistant Professor Deanna Hence

ABSTRACT

The vertical wind shear (VWS) within the tropical cyclone (TC) environment is a crucial factor affecting the track and intensity of the TCs. Classic theories in the 1950s proposed that weaker vertical wind shear favors the development of TCs. Several studies have been long investigating the physical linkages between the VWS and TCs. However, TC vertical wind shear is essentially a part of the larger environment, subject to the background fields and synoptic configurations. Research about how the large-scale environmental fields adjust and influence the VWS and TC properties is limited and incomplete. In this study, we perform a cluster analysis to understand how the synoptic configurations affect the pattern of VWS, and what influence they have on TC activities in the Western North Pacific.

A machine learning method, "self-organizing maps" (SOMs) is applied in this study to identify and discriminate the meteorological patterns in TC environment. A sample of 309 storms during 2010 - 2019 were examined, and several factors were used for SOM training. By inspecting the characteristics of other variables corresponding to these patterns, this thesis encompasses the discussion of TC time distribution, evolvement, environmental VWS, and large-scale environment, where evident correlation between these variables is found and revealed. The development of TCs is demonstrated in an evolutional manner, where the presence and state of the major weather systems in this area such as Western North Pacific Subtropical High (WNPSH), South Asian High (SAH), and monsoon gyre are closely related to the separate stages of TCs and invoke TC variations.

Keywords: Tropical Cyclone; Western North Pacific; Environment; Self-Organizing Maps

ACKNOWLEDGMENTS

I am very thankful to my family, friends, as well as the guidance of my advisors.

I have not suffered much in my twenty-three years of life, and I have relied on the help of various people to get to this point, which is certainly a blessing. However, the more I explore, the more I find that we are entangled in bondage and shackles, and at the very start of my life journey, I feel shallow and weak. If I don't try, the fire in my heart will be extinguished and I will be no different from caged livestock. I must keep going, to encourage myself.

TABLE OF CONTENTS

CHAPTER 1: INTRODUCTION

Tropical cyclones (TCs) are one of the most disastrous weather systems on the earth. Among the basins where tropical cyclones are likely to happen, almost one-third of the annual tropical cyclones occur in the western North Pacific (WNP) basin (NOAA, 2017), the most active basin on the planet. One of the deadliest typhoons (a strong and mature tropical cyclone in the northwestern Pacific basin) named "Haiyan" struck the Philippines in 2014 and caused 6300 deaths in this country alone (NDRRMC, 2014).

In recent decades, the ability of TC track forecasting has dramatically improved due to:

- The improved understanding of the physical processes and mechanisms of TC motion (Wang et al. 1998; Emanuel, 2000).
- The advances in numerical models (Kurihara et al. 1998), data assimilation systems (Guo et al. 2000; Pu and Braun, 2001) and adaptive observations (Aberson, 2003; Wu et al. 2006).
- The abundance of accurate satellite and remotely sensed data (Aberson, 2002; Wu et al. 2007).

In contrast, the forecast accuracy for TC intensity has almost stagnated (Harnos and Nesbitt, 2011; Tallapragada et al. 2014), especially at the 5-day lead time (Kieu, 2021). The fundamental reasons are:

- The lack of ocean surface observational data (Cangialosi and Franklin, 2012; Tallapragada et al. 2014),
- The inaccurate initial field and low resolution in modeling (Knaff et al. 2007, DeMaria et al. 2014).

- The incomplete understanding of the complex physical processes influencing TC intensity change (Zhang et al. 2015).

Wang and Wu (2004); Houze et al. (2006) have pointed out that the TC physical processes include subsurface forcing, internal thermodynamic processes at the ocean surface, thermodynamic and kinematic processes within the TC inner core and rainbands, and environmental field-TC interactions.

In the division of environmental field-TC interactions, vertical wind shear has been considered one of the significant environmental factors affecting the development of TCs and other mesoscale convective systems. Newton (1950) first proposed a conceptual model of vertical wind shear affecting thunderstorms, suggesting that the spiral circulation caused by the imbalance between the vertical shear of the ambient wind and the "thermal wind" enhances the configuration of low-level convergence and high-level dispersion that favors storm development. Gray (1968) reported that most tropical cyclones form in low-latitude regions where the vertical wind shear is a minimum or zero. DeMaria (1996), Wong and Chan (2004) demonstrated through statistics and data simulations that vertical wind shear and tropical storm intensification are negatively correlated, and weak vertical wind shear is essential for TC generation and development, which became the mainstream view in the state-of-the-art. Part of the reason is that the VWS adjusts the warm-core structure, which is associated with the strength of the primary circulation (Franklin et al. 2003) and the cyclone's intensity (e.g., Komaromi and Doyle, 2017).

Additionally, the loss of diabatic heat and the involvement of lower-entropy air into the downshear updrafts on the lower level was confirmed to be possible results of strong VWS (Finocchio et al. 2021). These effects strongly prevent the intensification or even drive the weakening process of the storms. Chen et al. (2021) proposed that the low-level mean flow

(LMF) associates the VWS and TCs as the air mass carrying high surface flux invades the downshear right quadrant facilitating the formation of rainbands, and a friction boundary inflow in the downshear quadrants promotes an asymmetric distribution of equivalent temperature in the inner core.

The above research explains the physical processes within the TC region. Nonetheless, the vertical wind shear, essentially the wind configuration, is a part of the large-scale environment. The study of the large-scale environments on TC intensity change enables us to understand the background and formation of wind/VWS and its impact on TCs from a dynamic perspective. As Holland (1984) described, the environment impacts the intensity, strength, and size of TCs. For the WNP basin, several significant weather systems are dominant in affecting the meteorological fields in this region, namely the Western North Pacific Subtropical High (WNPSH; e.g., Shu et al. 2013; Shu et al. 2014, Wu et al. 2020), South Asian High (SAH; Wang and Wang, 2021), and monsoon gyre (e.g., Lander 1994). Hu et al. (2020) found that the early (or late) withdrawal of the South China Sea summer monsoon affects the activity of TC genesis through dynamic (Rossby wave response) and thermodynamic (moisture) processes. However, their analysis is only based on a single system, and no joint analysis of the three effects was conducted. Therefore, it is crucial to perform a joint analysis covering all the systems, which is the motivation of this research: to determine the effect of weather configurations on TCs over WNP.

The intensity change within the distribution tail is less characterized by traditional statistical forecasting methods (Harnos and Nesbitt, 2016), thus a challenge for obtaining skillful TC intensity forecasts. Defined by Kaplan and DeMaria (2003), RI is a maximum sustained surface wind speed increase of 15.4 m/s (30 kt) over a 24-h period, representing about 95

percentile of over-water 24-h intensity change. They proposed that storms undergoing rapid intensification (RI) are likely more severe than those without RI. As one of the most unpredictable processes of TCs (Shu et al, 2012), understanding RI is vital to operation and research. Although commonly acknowledged environmental factors are postulated, such as sea surface temperature (SST), vertical wind shear (VWS), and relative humidity (RH), the weather systems' interaction with RI is not yet clear.

Similarly, rapid weakening (RW) is the stage where TCs rapidly decays in a 24-h period. For convenience, this study defines RI as a 15-m/s or more increase in the maximum sustained wind speed and RW as a 15-m/s or more decrease in the maximum sustained wind speed. Again, we are curious about what forms these conditions and TC interactions with critical weather systems in WNP.

In past studies, cluster analysis has effectively recognized distinct groups of atmosphere circulation states in atmospheric sciences. One of the clustering approaches, Self-Organizing Maps (SOMs), is distinguished for its unique ability to retrieve relevant and distinct atmospheric conditions. Traditional clustering methods such as hierarchical clustering, K-means, and Gaussian mixtures (Hannachi, 2017) are based on a numerical calculation to slice and split the data into clusters. In contrast, SOMs account for the whole data space and find the representations by the "best match". With the advantage of capturing non-linear characteristics, SOMs are favored for weather classification that is complex and undefined. Lennard and Hegerl (2015) used SOMs to retrieve the synoptic fields related to the surface rainfall response. Kim and Seo (2016) used SOMs to identify the different patterns of TC tracks over the WNP basin. Future changes in TC genesis locations and frequency were explored by relating to large-scale patterns using SOMs in the work by Jaye et al (2019). TC tracks were divided into 16 clusters, and SOMs

helped allow flood forecasts up to two days in advance (Chang et al, 2020). Based on the experience of previous studies, the SOMs can identify patterns of TC environmental fields and relate them to variables at various scales, which applies to this study.

CHAPTER 2: DATA AND METHODOLOGY

2.1 DATA

The cyclone data, including intensity, occurrence time, center latitude, and center longitude, is archived from International Best Track Archive for Climate Stewardship (IBTrACS) from NOAA. This research examines 309 storms between 2010 and 2019, recorded for each six-hour interval, amounting to 8190 records. Since tropical cyclones degenerate into extratropical cyclones when they move north of 35 degrees N, the records of TCs above this latitude were not counted to ensure the tropical cyclone properties are present. The statistics of some information of TCs are shown in Fig. 1 and Fig. 2.

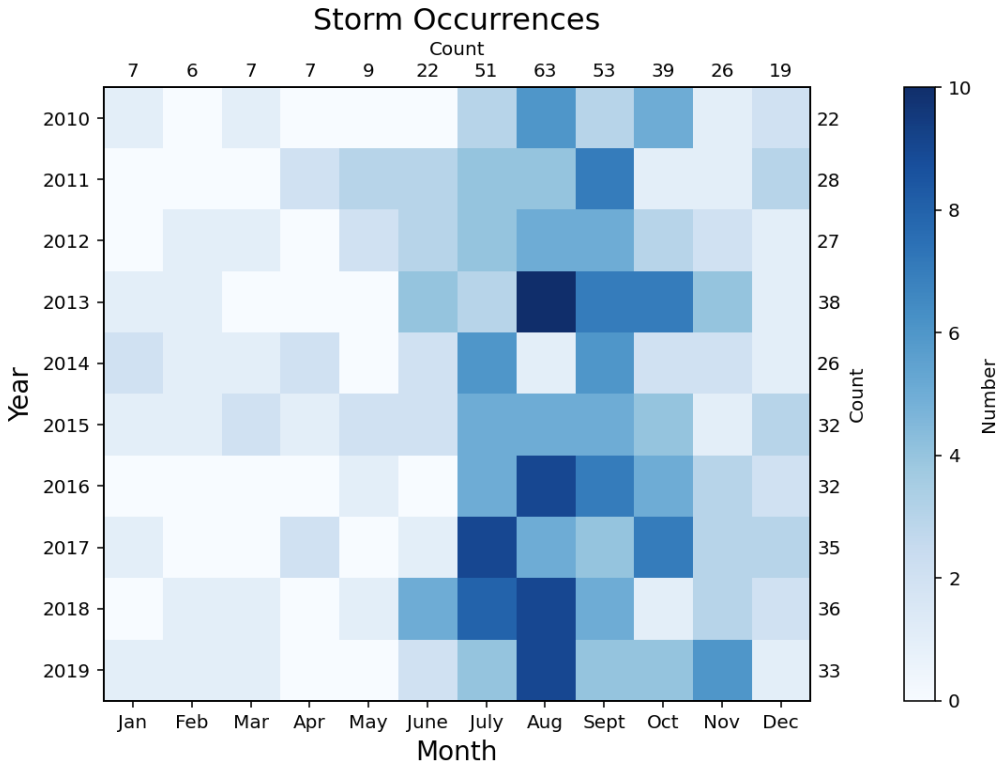

FIG. 1. Heatmap for TC occurrences arranged by year and month. The number on the right is the sum of the year, and the number on the top is the sum for the given month throughout the study.

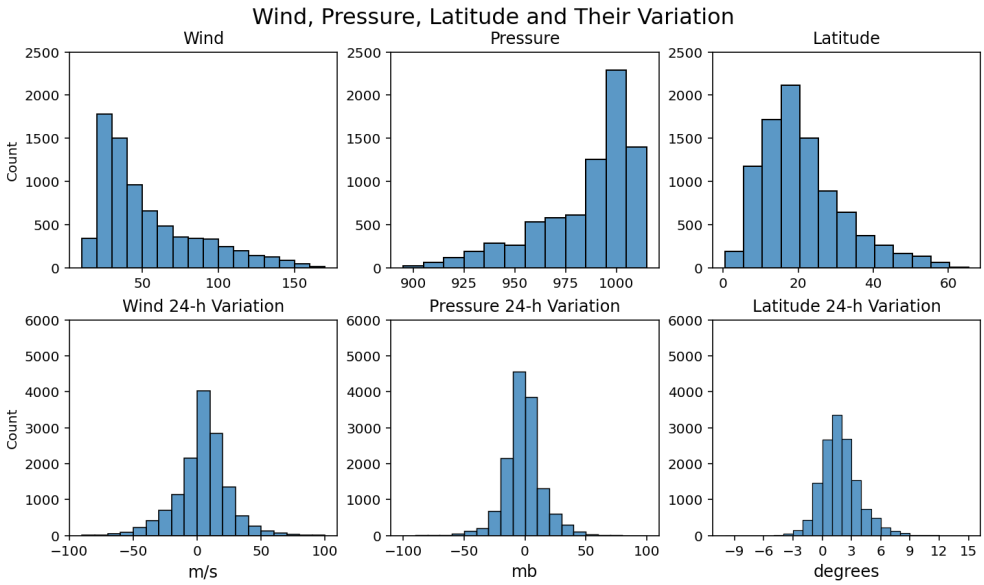

FIG. 2. Distribution of TC maixmum sustained wind, center pressure, center latitude and their changes.

The 6-hourly, 1°x1° FNL Operational Model Global Tropospheric Analyses from NCEP were utilized to retrieve the meteorological fields. The variables sourced from this dataset are zonal wind, meridional wind, and temperature on multiple layers, selected at the time of tropical cyclone occurrences based on IBTrACS data.

The variables appearing in this research are listed in Table 1:

TABLE 1. Variables and codes

Source	Code and Unit	Variable
NOAA IBTrACS	Wind (m/s)	Maximum sustained wind speed recorded by USA agency
	Pressure (mb)	Minimum central pressure recorded by USA agency
	Lon (degrees)	Longitude of tropical cyclone centroids
	Lat (degrees)	Latitude of tropical cyclone centroids

TABLE 1. Variables and codes (Cont.)

Source	Code and Unit	Variable
NCEP FNL	U 850 (m/s)	Zonal wind on 850 hPa
	U 850 (m/s)	Zonal wind on 500 hPa
	U 200 (m/s)	Zonal wind on 200 hPa
	V 850 (m/s)	Meridional wind on 850 hPa
	V 500 (m/s)	Meridional wind on 500 hPa
	V 200 (m/s)	Meridional wind on 200 hPa
	GPH 850 (m)	Geopotential height on 850 hPa
	GPH 500 (m)	Geopotential height on 500 hPa
	GPH 200 (m)	Geopotential height on 200 hPa

2.2 Self-Organizing Maps

A Self-Organizing Map (Teuvo Kohonen, 1982) is a powerful unsupervised machine learning technique featuring data mining. By projecting high-dimensional data on a two-dimensional map while reserving the topological structure, it provides a simple representation of the original data that is easy to read and interpret. Compared to other clustering methods, The organization and learning process is briefly described as follows. A SOM has two layers: the input layer for data samples, and the output layer consisting of x (artificially defined number) nodes, known as clusters. Each node is a vector with y components called “weights”, where y is the size of the first dimension of the input. The nodes are initialized by random or specific values, which do not affect the results of the training. By computing the Euclidean distance between the input vector and each node, the SOM finds the closest node to the input, which is the

"best matching unit (BMU)". Finding the BMU, the SOM will update its "weights" to be closer to the input. When the weights of one node are updated, it will also draw the nearby nodes closer. With the ultimate goal of aligning the map with the samples, the iterative process will go through the entire input data space and make sure the overall quantization error (distance between input and output vectors) is minimum. By the end of the training, the x nodes (clusters) represent x patterns in the input dataset, where distinct characteristics are exhibited, and similarities may also exist. For detailed information, refer to "The Ultimate Guide to Self-Organizing Maps (SOMs)" (SuperDataScience Team, 2018).

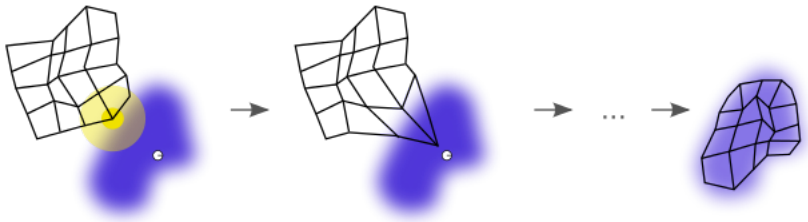

FIG. 3. The blue region is the input data, where the white dot is an input vector. At first (left) the nodes of the map are randomly distributed, when the BMU is determined for the input vector. The BMU is pulled closer to the input vector, as are the nearby nodes (middle). The process is iterated for other input samples until the map aligns with the training data (right). (adapted from Mcld, 2010)

2.3 SOM input and training

This study aims to understand the effect of synoptic configurations on TCs over the WNP. In brief, the methodology is to use SOM to train on the TC environmental variables and investigate the relationships of those variables as well as TC characteristics in each cluster with other variables. Multiple variables were used for SOM training, and geopotential height at 500 hPa (GPH 500 hPa) outperforms zonal wind, meridional wind, and wind shear for having the

highest silhouette coefficient (0.357, describing how well the clusters are apart from each other). Therefore, we chose the geopotential height on 500 hPa (GPH 500 hPa) as our training variable, exemplifying the mid-level mass field and circulation state. As mentioned in the previous section, 8190 samples are involved in this study. The first step is to select all the GPH 500 hPa samples from the region that is dynamically relative to the TC center. In the literature, the TC environment is defined as the area within 800 km of TC center, around 8 degrees lat/lon. Therefore, a 16-degrees-by-16-degrees grid box centered on the TC centroid is applied in this project for data training and presentation.

Then a Z-score normalization is first performed within each sample. After the training data is all prepared, the SOM will be used to train the data. We used the *minisom* python package, with credit to Giuseppe Vettigli (2018) on Github. The SOM was set to have 4, 6, 8, 9, 12, and 16 nodes in our individual experiments, among which nine nodes ended up showing the ability to best describe distinct weather patterns. Nine clusters of weather patterns are identified, discriminated, and recovered. Each cluster represents a certain number of samples, and each sample is assigned a "cluster index," referring to the cluster it belongs to.

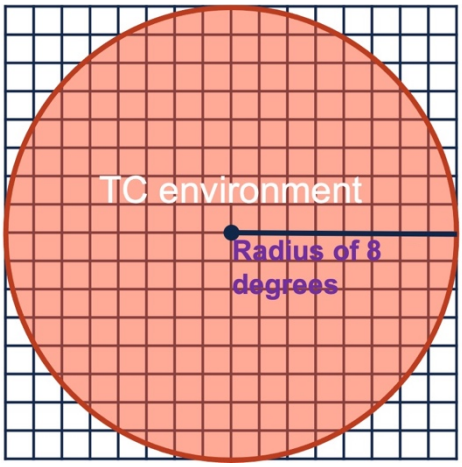

FIG. 4. Schematic of input format. The TC environment is denoted in the orange circle, and the input space is distributed in the 16-degrees-by-16-degrees grid points in the black matrix.

CHAPTER 3: CLUSTERING RESULTS: GPH 500 hPa PATTERNS

The results from SOM training are processed and visualized in Fig. 5. Every panel exhibits the composite of GPH 500 hPa patterns for each cluster, respectively. Various patterns are observed, where the gaps between the clusters suggest that SOMs successfully discriminated GPH 500 hPa field patterns. Here we provide simple descriptions for each cluster.

Clusters 1 and 4 both have high overall GPH 500 hPa considering the distribution of the whole basin, whereas cluster 4 has even higher GPH, especially in the northeast part. Cluster 2 has very low pressure at the center and high pressure at the northeast corner, showing a strong contrast between the core and outside region while maintaining a relatively symmetrical structure in the core area. Following gradient wind balance, it is hypothesized that this cluster reveals that the stronger gradient in the cluster mean, the more intense the statistical distribution of TC intensities is likely to be. This will be revisited below.

Cluster 3 is characterized by a weaker low center (higher GPH). The air pressure in the east is higher than in the west, forming an eastern semicircle surrounding TC in the center, and the air pressure decreases from east to west.

Cluster 5 is also connected with a very low-pressure center like cluster 2. However, the pressure in the region distant from the TC is not as high as in cluster 2, suggesting a lower contrast between the core and environment. Like cluster 3, the high pressure in cluster 5 forms a semicircle on the east edge of the TC range.

Clusters 6 to 9 differ internally, but the overall characteristics are relatively similar. The typical features of clusters 6 to 9 are that the symmetric structure no longer exists. However, there is a gradient of air pressure decreasing from southeast to northwest in the general

environment. Amongst them, cluster 6 approximates cluster 5 with a deep, sizable low-pressure center, whereas cluster 7 has a weak, small center embedded in a high-pressure environment. In cluster 8, the isolated low-pressure center structure is barely visible. In cluster 9, the low-pressure center of TC is connected to the low pressure in a wide area to the north. These clusters resemble a mid-latitude cyclone pattern, with a TC possibly undergoing or soon to undergo extratropical transition.

We have observed the similarities and differences among these clusters, where their distinct features are presented. We believe that the orientation and organization of these GPH patterns are associated with certain TC activities and patterns or environmental factors. To understand how different GPH patterns are related to TC characteristics, behavior, and environmental fields, we will compare other variables that are concurrent with these clusters to explore the mutual relationships among them.

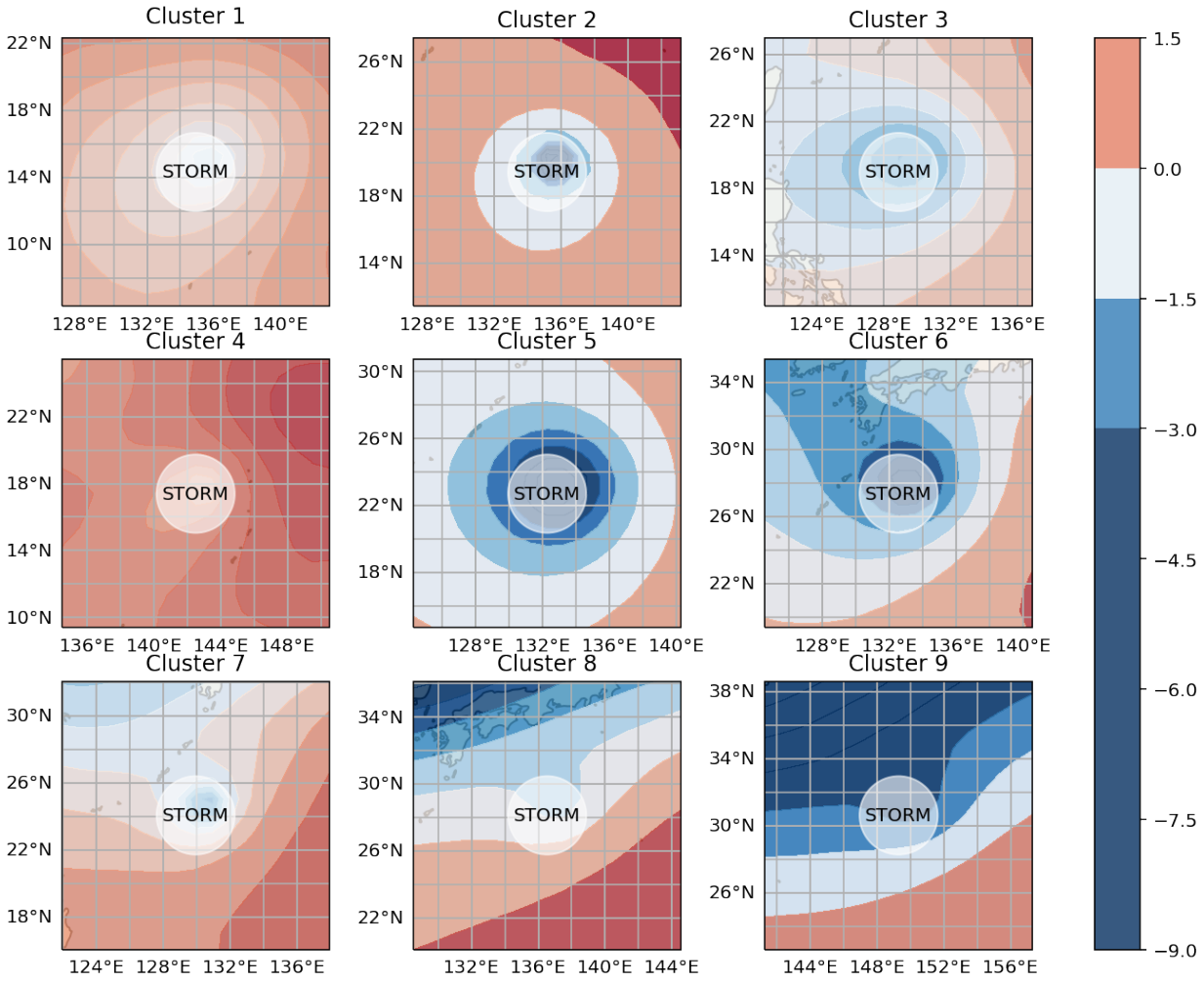

FIG. 5. Storm-relative Z-score normalized GPH 500 hPa patterns. The average location of the TC centroid is at the center of the graph; the longitude and latitude are organized based on the coordinates of TC centroids (same for the rest of maps appeared in this chapter). Red colors are GPH higher than average; blue colors are GPH lower than average.

CHAPTER 4: TC TIME DISTRIBUTION, STAGE, INTENSITY, AND INTENSITY CHANGE

In this chapter, we will examine how different clusters are associated with different TC characteristics.

4.1 Month distribution

Fig. 6 shows the time distribution of TC samples in months over the year. Note that the sample size within each cluster is not necessarily the same. The cluster with the largest sample size is cluster 1 (3102 samples), whereas clusters 3 (1493 samples) and 4 (1239 samples) are the second and third largest-sample-size clusters, respectively. Other clusters have less than 1000 samples each. Temporally, the concentration of samples from July to October (known as typhoon season) is the most distinguishing feature in the five clusters from 1 to 5. Due to the high frequency of TCs occurrences from July to October (known as the "typhoon season"), it is not surprising that the temporal distribution of some clusters focuses on this period. However, the rest of the clusters, 6 to 9, are more evenly distributed. Notably, most clusters have samples all over the year, suggesting that the GPH 500 hPa configuration in most clusters can occur throughout the year rather than being restricted to a particular season. Seasonality does be observed, but only in typhoon season.

The sample size represents how common each cluster is, and the time distribution reflects the seasonality of the TCs belonging to each cluster. Clusters 1, 3, and 4 are the most general conditions in TC activities, whose GPH 500 hPa are more explained in the summertime. Clusters 2 and 5 almost only occur in the summertime, so there are hardly any patterns of clusters 2 and 5

happening in non-typhoon seasons. Clusters 6 to 9 are the minorities describing the less-common scenarios that evenly distribute around the year.

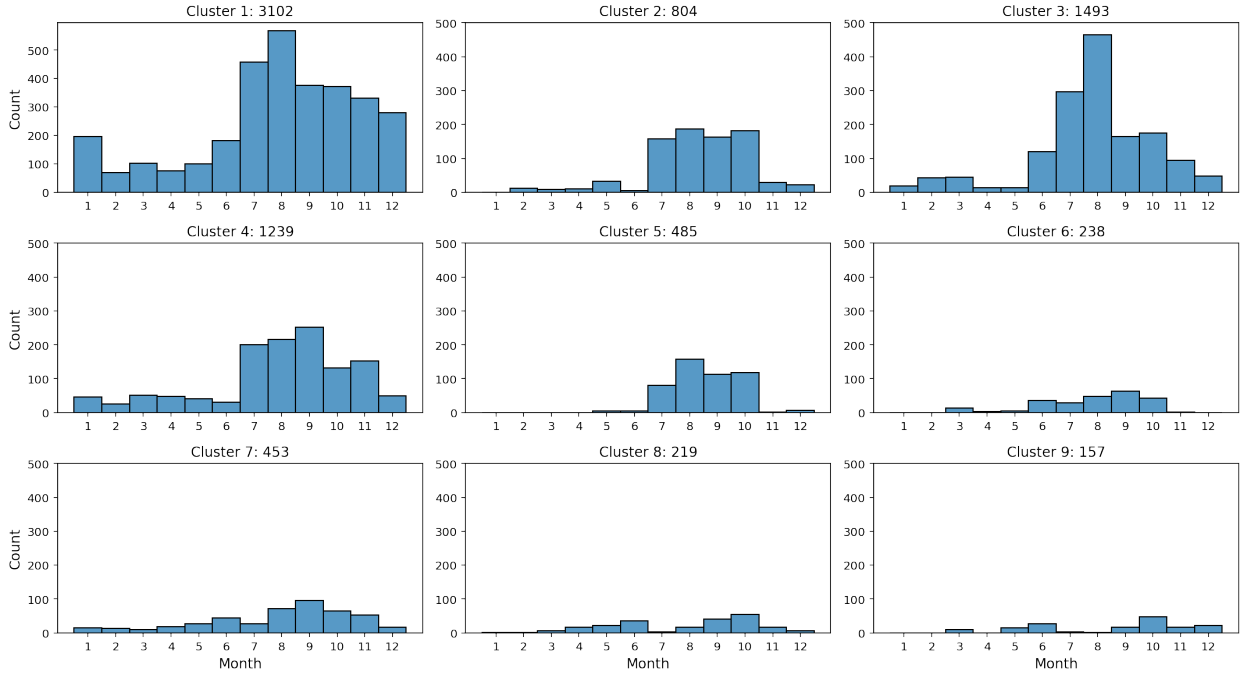

FIG. 6. Time distribution of TC samples in months. The x axis is the month; y axis is the number of occurrences.

4.2 Stage distributions

The tropical cyclone lifetime consists of four stages, i.e., formation, development, maturity, and depression. We believe that exploring whether clustering is related to TC life stages is greatly beneficial to this research because studying tropical cyclone stages enables us to understand the current nature of tropical cyclones and their subsequent actions. Fig. 7 exhibits the ratio of time since TC formation to overall lifetime in each cluster, which depicts the distribution of the relative stage of TCs. Although in this histogram, all clusters have samples in almost every bin, the differences in distribution can be captured. Clusters 1 and 4 are more of an earlier stage in TC lifetime. Cluster 2 focuses on the middle stage. Cluster 5 is from the middle to

late stage. Clusters 6 to 9 are significantly late stages. Cluster 3 shows evenness in the distribution, which indicates that it might be a transitional phase during TC lifetime. Therefore, we propose that clusters connect to the TC stage of phase.

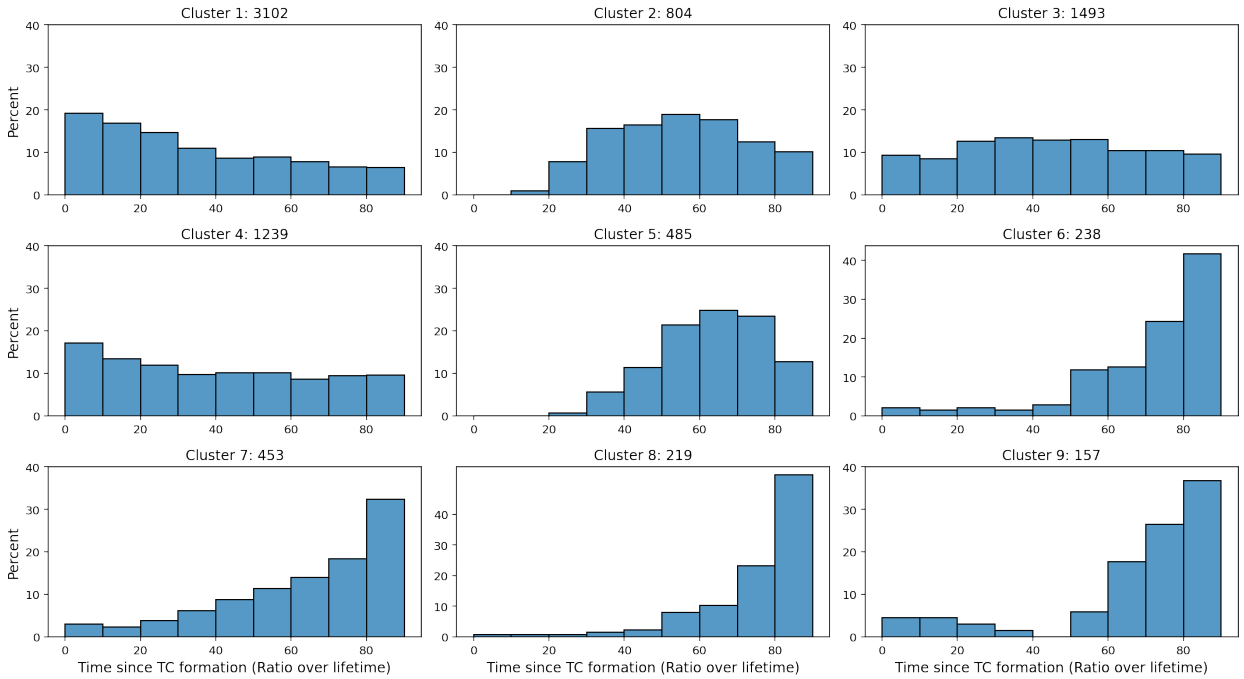

FIG. 7. The distribution of the ratio of time since TC formation over lifetime. The x axis is the time since TC formation (ratio over lifetime); y axis is the percentage of each bar relative to the whole cluster.

4.3 Intensity distribution

TC intensity is one of the most important attributes of tropical cyclones, and as discussed above, one of the most difficult to forecast. In Fig. 8, a distinct variability of TC intensity among clusters is observed. Cluster 1 and 4 show mostly a distribution of low TC intensity, with most of the samples between 10 and 20 m/s. Cluster 2 and 5 are characterized by higher mean values around 40 ~ 50 m/s and flatter distribution, which indicates high variance. Most of the remaining clusters are concentrated in the low-intensity portion, with a few high-intensity samples. The

difference in intensity suggests the variability of intensity can be captured and differentiated through SOM training on GPH 500 hPa. This is important because if we have captured a GPH 500 hPa environment around a TC that is similar to one of the nine clusters, we can use the intensity distribution of the clusters to make an approximate determination of the intensity range of the TC. Their correspondence is summarized as, generally speaking: cluster 1 and 4 are weak storms, cluster 2 and 5 are strong storms, and the rest are of moderate intensity.

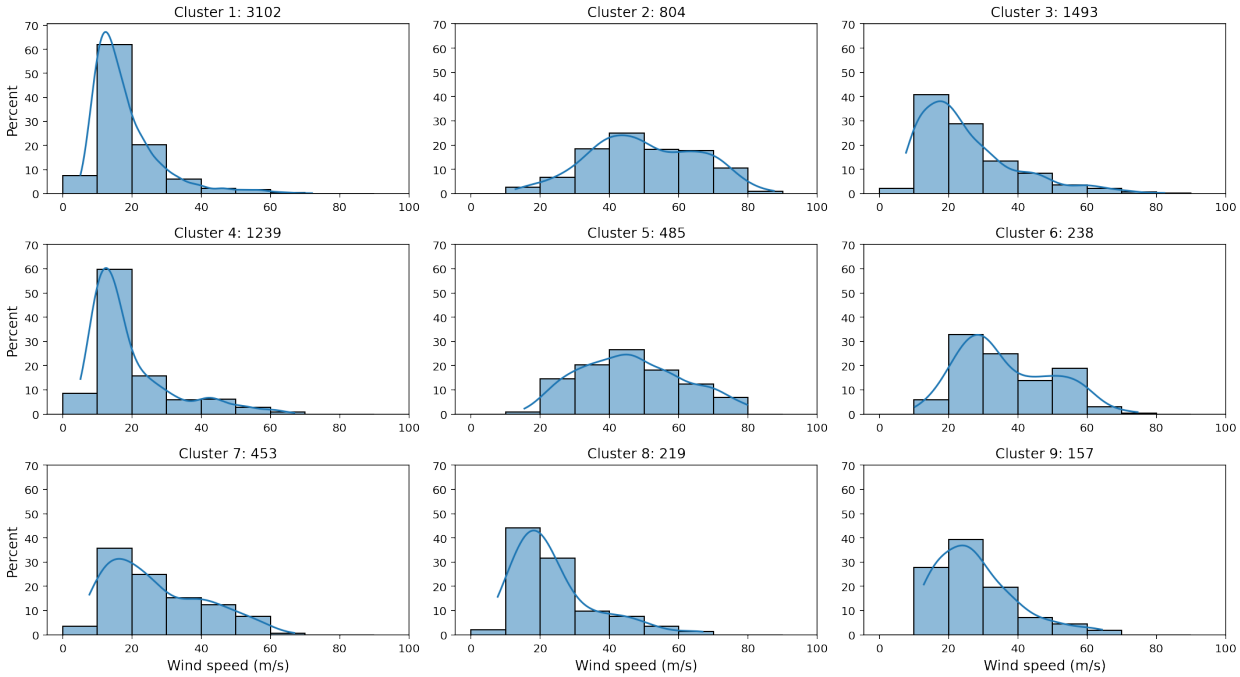

FIG. 8. Intensity distribution. The x axis is the wind speed (m/s); the y axis is the percentage of each bar over the cluster; the blue lines represent the kernel density estimation of wind speed.

4.4 Intensity change distribution

In prediction, intensity change is usually defined as the maximum sustained wind speed change in a 24 hours, adopted in this work for examination. The intensity changes are categorized into four groups: slow intensification (SI, 0 ~ 15 m/s), rapid intensification (RI, > 15 m/s), slow weakening (SW, -15 ~ 0 m/s), and rapid weakening (RW, < -15m/s).

Fig. 9 displays the intensity change distribution. Like the intensity histogram, this figure shows significant gaps between clusters 1, 4 and clusters 2, 5. Clusters 1 and 4 mainly focus on SW, with 90 percent of the distribution having slow intensity changes. In contrast, in clusters 2 and 5, only 67.9% and 80.2% slow-changing rates are found. Those higher rates indicate the stability of the storms, whereas the higher rates of RI and RW suggest that the storms are more unstable, fast-changing, and potentially difficult to predict. However, it is notable that differences exist between clusters 2 and 5. Cluster 2 has both high RW rate (18.7%) and RI rate (13.4%), while cluster 5 has a high RW rate (17.2%) and a low RI rate (2.6%). If we recall the stages of TC lifetime these clusters are in, cluster 2 is more of a middle stage, while cluster 5 is from middle to late stage. It intuitively explains why cluster 2 may either rapidly intensify or weaken. In contrast, cluster 5 is more likely to rapidly weaken due to the greater likelihood of associating with making landfall, moving out of a favorable meteorological condition, or extratropical transition. Nonetheless, it is interesting to see high RI and RW rates both exist in cluster 2, manifesting great unpredictability. Since the GPH 500 hPa configuration is similar for all samples in cluster 2, understanding the factor that causes this difference is the key. Therefore, in more detail, we will investigate cluster 2 and discuss it in chapter 7.

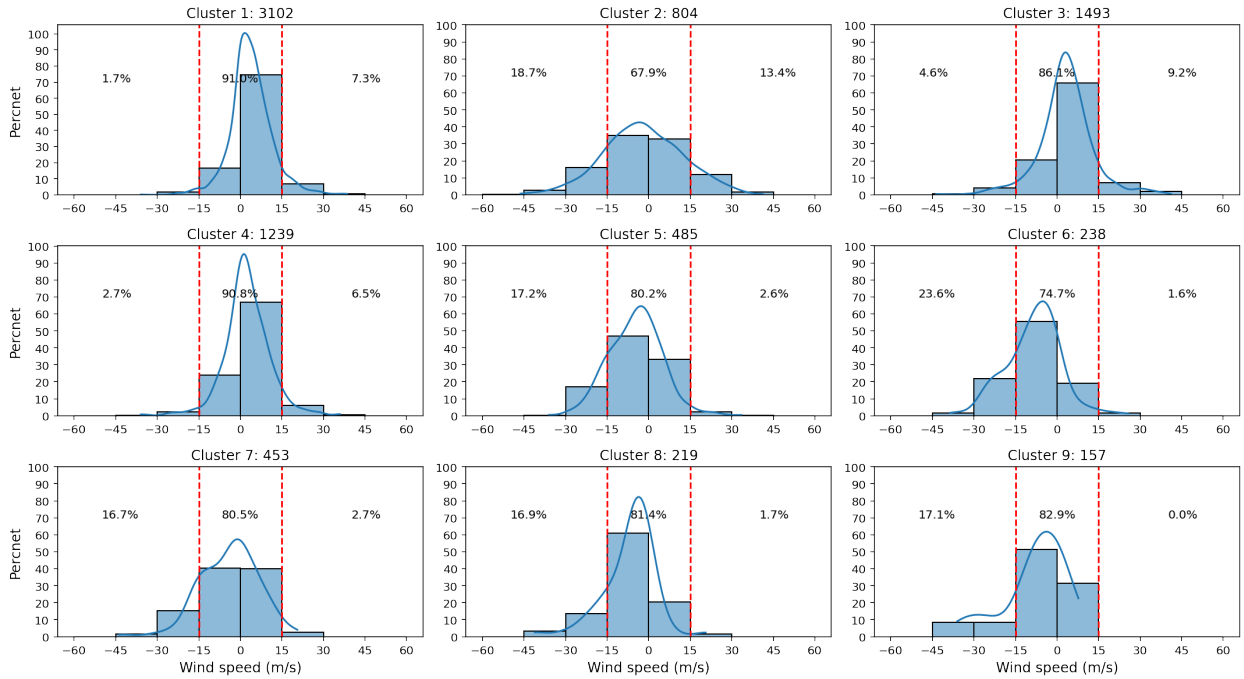

FIG. 9. Intensity change distribution. The blue lines represent the kernel density estimation of intensity. The right red dashed line is threshold for rapid intensification (>15 m/s), the left red dashed line is threshold for rapid weakening (<-15 m/s). The numbers in the graph represent RW rate, non-RI or RW rate, and RI rate.

4.5 Summary

In this chapter, we discussed the temporal distribution, phase distribution, intensity, and intensity variation information of WP TCs in each cluster. Each cluster has unique characteristics; the differences between the clusters are apparent. We summarize the findings as follows:

Clusters 1 and 4 are weak, stable storms that are often in the earlier stages of their lifetime. Cluster 2 is strong storms with high unpredictability in the middle stage. Cluster 5 represents intense storms likely to depress from middle to late stage rapidly. Clusters 6 to 9 all reflect late-stage storms. Cluster 3 seems to be a transition phase between clusters. In the

following chapters of this paper, we will continue to follow the sequence of clusters 1 and 4, clusters 2 and 5, clusters 6 to 9, and cluster 3 to discuss.

CHAPTER 5: SYNOPTIC CONFIGURATIONS AND RELATION TO TC CHARACTERISTICS

5.1 Composite analysis of 850 hPa fields

In chapter 4, we discussed the characteristics of TCs in each cluster. As is known, synoptic configurations have a significant impact on TC behaviors. In this chapter, we will continue investigating the composite large-scale environmental fields corresponding to all clusters and how they relate to the TC characteristics.

Fig. 10 shows the mean large-scale environmental wind and GPH field on 850 hPa with TC average location marked in the orange circle. All the discussion in this chapter represents the situation regarding the intermediate state of tropical cyclones and environmental fields; all fields are displayed as centered on that location.

The average location for cluster 1 is around 133 degrees E, 15 degrees N, consistent with the earlier onset characteristics. The 1500 m isohypse extends straight from southeast to northwest into mainland China. The high-pressure system characterized by a 1540 m isohypse is far from the TC, at more than 15 degrees latitude/longitude. In cluster 4, the TC is affected by the easterly flow to the south of the high-pressure system only. The TC whose location coincides with 1520 m isohypse is under an overall higher-pressure background. The 1500 m isohypse encloses a vast area east of 110 degrees E and south of around 38 degrees N.

In cluster 2, the TC located at the intersection of the two flow streams is affected by a robust east-southeasterly flow and a weak southwesterly flow, which is the monsoon flow that occurs in monsoon seasons. In cluster 5, the TC is involved in the fast-rotating monsoon gyre characterized by a low-pressure center over the Philippines Sea, sitting near its eastern flank. The

inflow of TC comes from the southwesterly flow. The high-pressure system to the east is distant, and the easterly flow moves northwestward along the eastern edge of the gyre without entering it. In clusters 6 to 9, the average locations of the TCs are above 25 degrees N. The TC in cluster 6 is to the south of Japan within a short distance, affected by a weakened northward monsoon gyre. The high-pressure system is so weak that the 1540 m isohypse disappears in this scenario. Cluster 7 has a similar GPH 850 hPa pattern to cluster 4 but a lower background pressure, with the 1500 m isohypse moving backward to the southeast. Compared to cluster 4, the average position of TC shifts roughly five longitudes and latitudes to the west and north, respectively. In cluster 8, the TC continues to move northeastward to around 30 degrees N along the 1500 m isohypse while the high-pressure retreat to the west. In cluster 9, the TC around 30 degrees N is caught in the westerly jet downstream of the trough.

In this part, we investigated the synoptic field on 850 hPa for the clusters of TCs to occur. Also, some speculative connections can be found and established between clusters. Cluster 6 evolved from cluster 5, and clusters 4, 7, and 8 follow the sequence. In the ensuing discussion, we will explore the connection between weather fields on other layers and TCs, and observe whether such relationships exist.

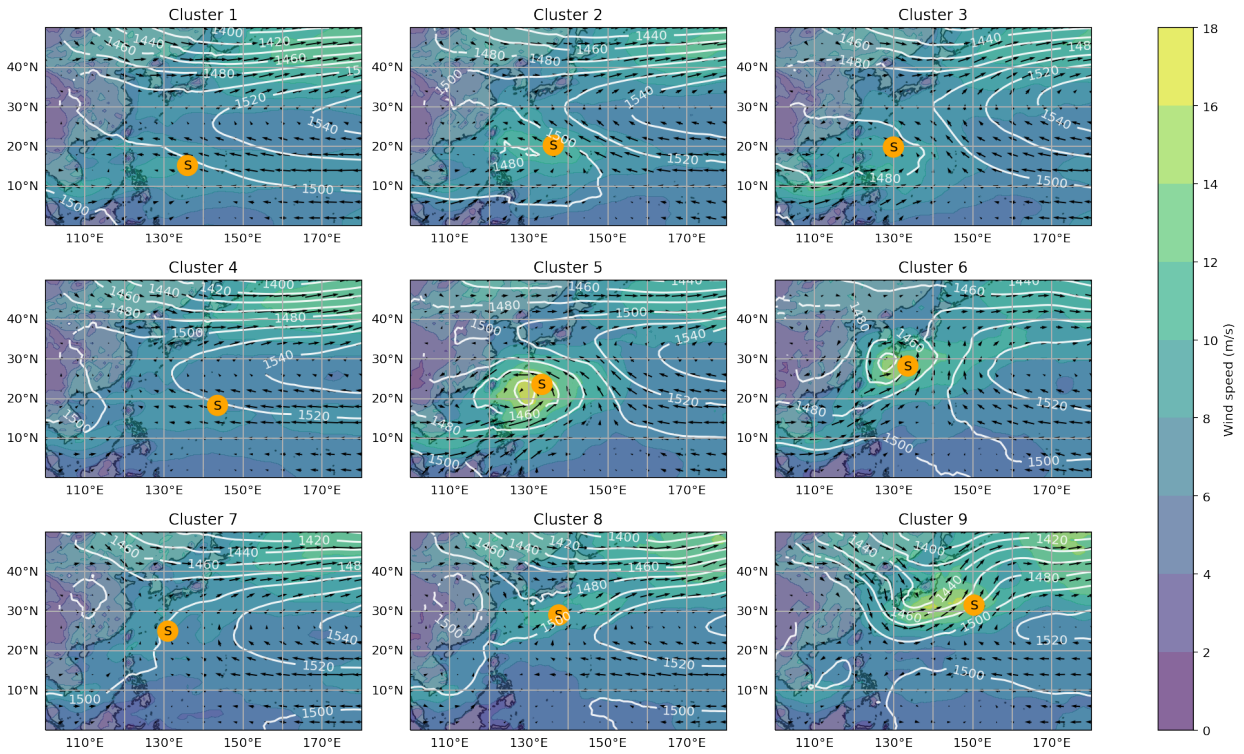

FIG. 10. Composite maps of 850 hPa wind (shaded, m/s and barbs) and GPH (contour, hPa).

5.2 Composite analysis of 500 hPa fields

At 500 hPa, the most influential weather system is the Western North Pacific Subtropical High (WNPSH). It is characterized here by the 5880 m isohypse, whose enclosing area reflects the strength of the High in terms of size and location. The connection between TC and WNPSH has been established. For example, Wu et al. (2005) found that the westward expansion and strengthening of the WNP subtropical high are responsible for the shifts of TC tracks due to the changes in the steering flow or the mean translation velocity. Ling et al. (2015) explained that the movement of WNPSH changes the vorticity, vertical wind shear, and convection conditions related to TC genesis. Nevertheless, most studies are focused on the TC tracks, while the relationship between TC intensity and WNPSH remains ambiguous. This section associates the previously obtained conclusions about intensity and intensity variation to 500 hPa patterns.

Cluster 1 is to the southwest of a weak WNPSH influenced by the clockwise circulation caused by high pressure. The background wind in the vicinity of the TC center is weak, around 6 - 12 m/s. In cluster 4, the TC is in the interior of a strong WNPSH extending to 120 degrees E, occupying a massively wide space. The wind inside the WNPSH is quasi-static due to a slight pressure gradient, which is consistent with what is shown here. The TC is under a low wind speed background of 6 - 9 m/s.

In cluster 2, the TC is on the southwest edge of the 5880 m isohypse, where the southeasterly flow from the south of the WNPSH is dominant. Compared to 850 hPa, the monsoon gyre is too weak to appear on 500 hPa; the TC is directed by the southeaster steering flow on both layers and will more accordingly. Cluster 5 differs from cluster 2 in a weak WNPSH and a powerful monsoon gyre forming a wide circulation on 500 hPa. Similar to the scenario of 850 hPa, the TC is precisely amid the strong gyre, while the WNPSH is too far away to have an effect. In cluster 6, the TC approaches the westerlies downstream of the deep trough over the East China Sea. The steering flow pushes the TC further northeast to the westerly jet. Recall the connection between clusters 5 and 6 from 850 hPa; we found a shallow trough in cluster 5, the upstream of the trough in cluster 6. On 850 hPa, the TC is involved in a weak low-pressure whirl, known as the gyre. The gyre is too weak to form a closed vortex, but with the eastward shift of the North China longwave trough, two low-pressure systems converge on the East China Sea to form an intense trough on 500 hPa, which is the dominant weather system for this cluster.

Clusters 7 and 8 are similar at 500 hPa. They are both on the northwest side of a strong WNPSH and in the vicinity of westerlies. In this configuration, the westerly flow formed by the two systems together pushes the TC eastward in a direction more parallel to the latitude line. In

cluster 9, the TC has gone into the westerly jet and the WNPSH vanishes, where late stages are expected. At last, in cluster 3, although the characteristics of WNPSH and monsoon flow can be observed in the motion of background air, no strong WNPSH or westerly trough is present. The TC is in a mild pressure gradient area, located at 130 degrees E, 20 degrees N, and hundreds of kilometers away from land on average.

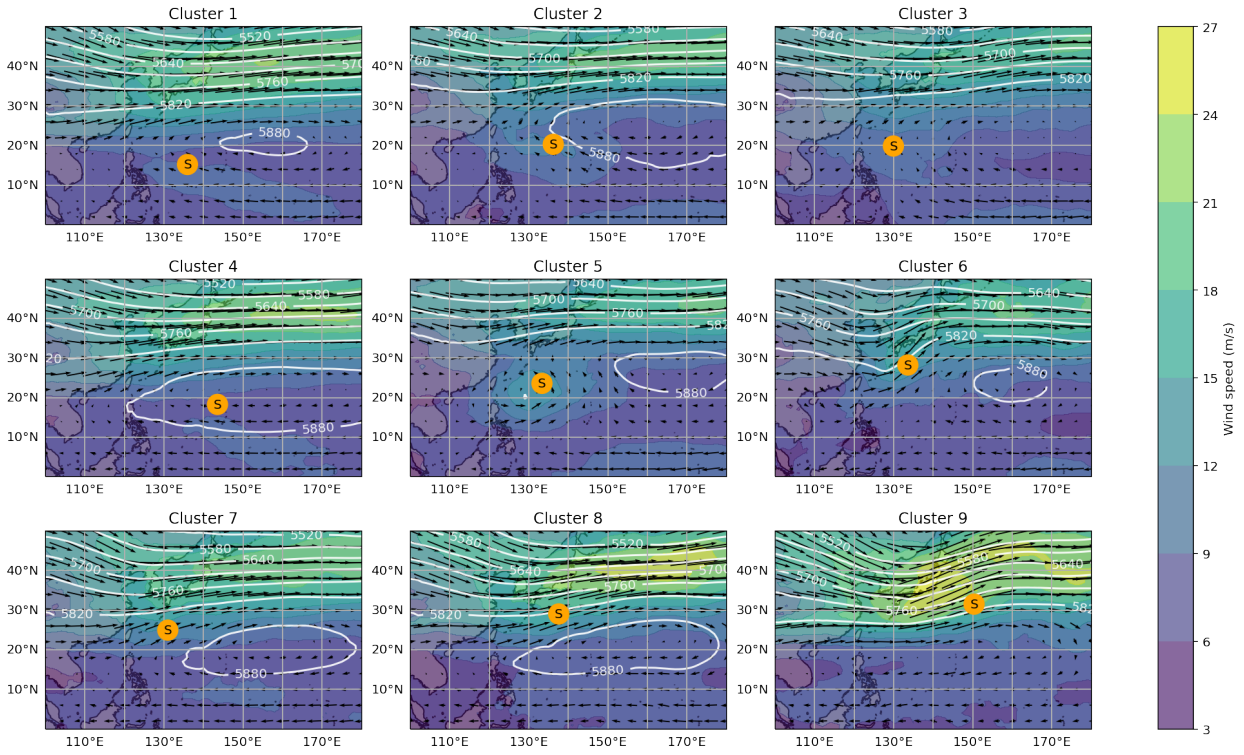

FIG. 11. Composite maps of 500 hPa wind (shaded, m/s and barbs) and GPH (contour, hPa).

5.3 Composite analysis of 200 hPa fields

It is known that the flow on the 200 hPa level impacts TC development (e.g., Sears and Velden, 2014) because of its relation to the upper-level warm core (e.g., Chen and Zhang, 2013). The previous discussion found that the lower and middle levels share similar background field patterns. At 200 hPa, the configurations could be quite different due to air circulation. In this

section, we will explore the upper level of the TC environment and see if the connections still apply in this situation.

The South Asian High (SAH) is a solid and persistent large-scale high-pressure system on the upper level that significantly impacts weather regimes in the Northern Hemisphere, including WNPTC. It is formed by the solid topographic uplift and thermal convergence forcing the ascent of air near the Tibetan Plateau. At 200 hPa, the SAH is characterized by the 12800 m isohypse.

In cluster 1, the SAH is so weak that it leaves the Asian continent and stays over the Pacific Ocean. The TC is on the southeast side of the counterclockwise circulation, influenced by the easterly-to-northeasterly flow. The wind speed around the TC is slow. In cluster 2, the SAH is intense, extending to 140 degrees E. The TC on the east edge of the 12800 hPa isohypse is in the northerly flow, slowly, as in cluster 1. In clusters 2 and 5, the TCs are surrounded by the robust SAH with similar intensity, where the environmental wind speed is low.

In contrast to the lower- and mid-level, the overall weather fields appear alike, although the SAH is slightly weaker in the cluster, and there is a small protrusion near 130° E. In clusters 6 to 8, the TCs are located between the SAH and westerlies, directed by the zonal westerly flow. In cluster 9, the 12800 hPa isohypse is not present, and the TC has entered the westerly jet stream. In cluster 3, the SAH is of medium strength among all clusters. The TC is about 3 degrees longitude east of the SAH, affected by the weak northwesterly flow.

In clusters 1 and 4, there is a clear correspondence between low-, middle- and high-level flows. A weak WNPSH corresponds to a weak SAH, and a strong WNPSH corresponds to a strong SAH. However, among all cases, the SAH has a similar intensity in 6 out of 9 clusters: clusters 2, 4, 5, 6, 7, and 8. The main difference between them is the location of the TC. This does not fully align with the lower- to mid-level, where a considerable gap is observed in GPH

and wind fields.

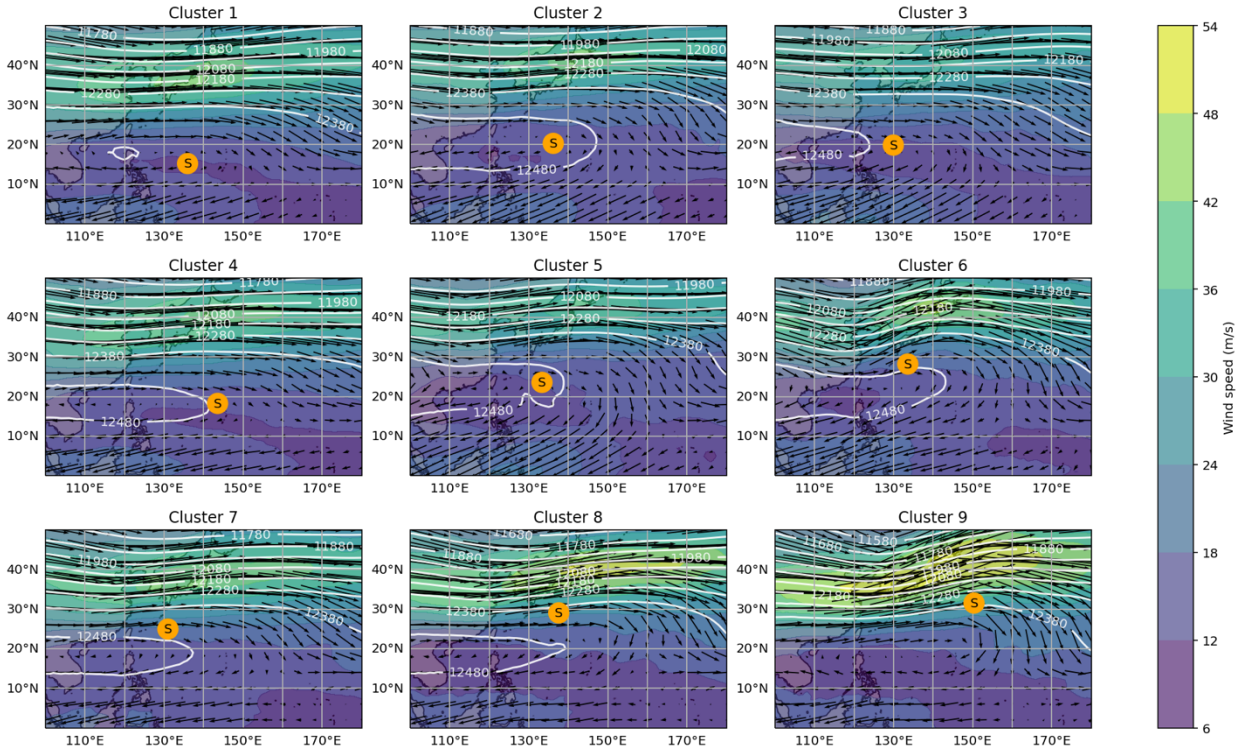

FIG. 12. Composite maps of 200 hPa wind (shaded, m/s and barbs) and GPH (contour, hPa).

5.4 Vertical wind shear patterns

Given the above weather patterns on different levels, we will examine the environmental vertical wind shear (VWS) fields that show the difference between upper and lower levels. The VWS has been widely demonstrated to influence the TC regarding intensity, intensity change, and tracks. Nonetheless, the past studies were primarily focused on the numerical calculation of composite mean VWS. Instead, we will present the whole VWS magnitude field for a clearer understanding. Because the VWS is usually studied in a storm-relative orientation, its visualization adopts the same method as the SOM training input. A 16-degrees-by-16-degrees grid box with a half side length approximating 800 km is consistent with the expected scale of studying VWS (e.g., Feng and Shu, 2018). The figure below shows the wind shear patterns

corresponding to each cluster. Clusters 1 and 4 have the lowest overall wind shear; clusters 2 and 5 are characterized by a high shear center. Clusters 6 to 9 have low shear on the south and very high shear on the north. Cluster 3 is still a transitional phase between low shear and high shear.

Relating to the conclusions obtained above, we found that during the early to middle stages, such as clusters 1 to 4, the VWS is generally low, favoring the slow intensification of TCs. In the intense scenario, the VWS, due to the circulation of the TC itself, forms a high shear center around the TC center. RI is also observed in this case since the environmental shear is still low. In the middle to late stage, as depicted in cluster 5, the shear grows in the outer band of TC, promoting the RW of TCs. In the late stages from clusters 6 to 9, the shear expands tremendously along with the dissipation of TCs.

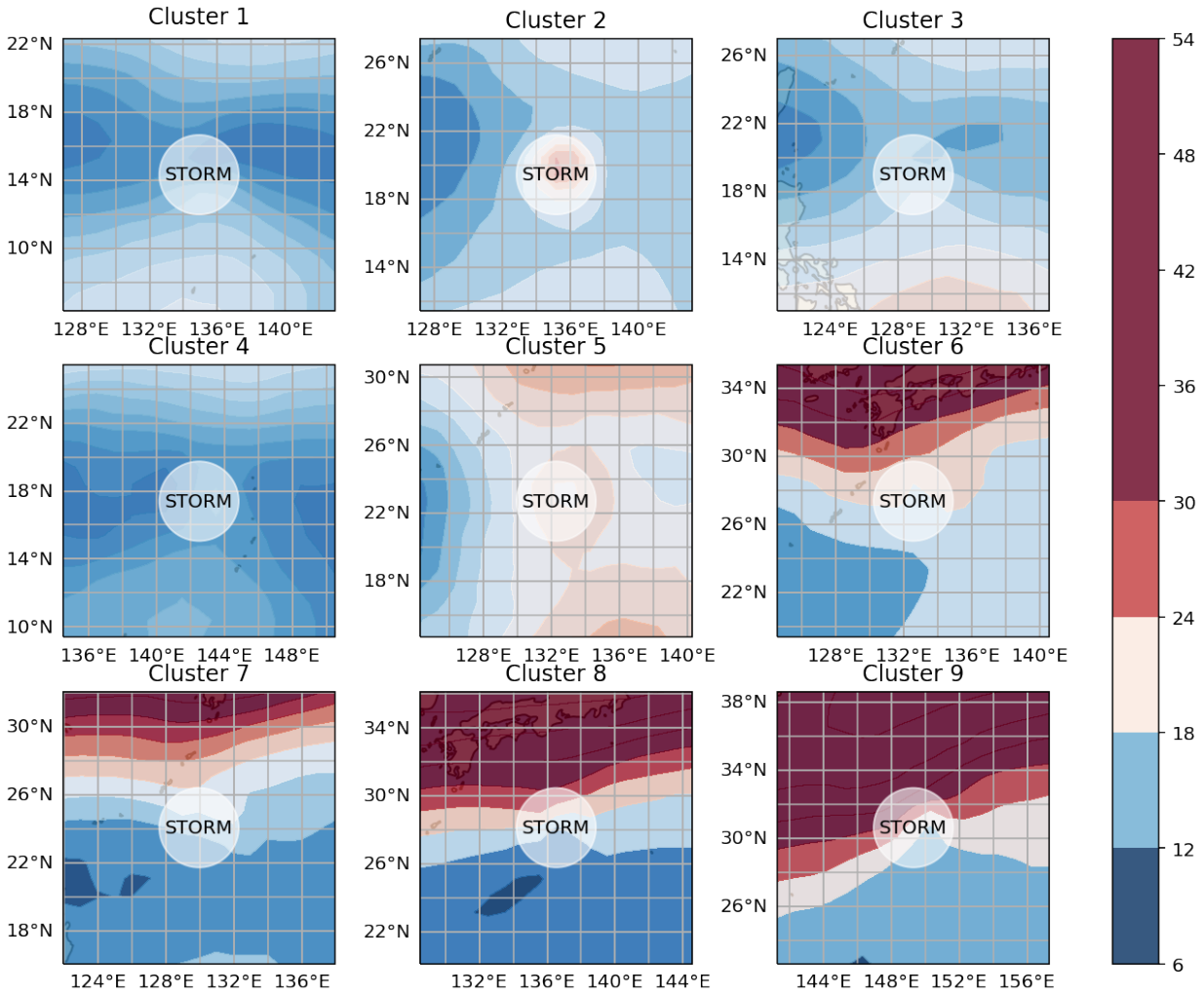

FIG. 13. Storm-relative total vertical wind shear magnitude. Red colors are wind shear magnitude higher than average; blue colors are wind shear magnitude lower than average.

5.5 Summary

This chapter focuses on the background configurations of 850 hPa, 500 hPa, and 200 hPa. Previous studies have revealed that the synoptic fields impact TC intensity. However, it is the first time we have distinguished up to nine TC modes and investigated the correlation with weather patterns behind each of them. We have established the background fields corresponding

to each cluster, representing a specific type of TC in terms of time, intensity, and intensity change.

The weak, stable, newly generated storms in clusters 1 and 4 are associated with only WNPSH and SAH. A weak SAH accompanies a weak WNPSH, and a strong WNPSH is affiliated with a strong WNPSH. Despite the gap in the intensity of the systems, the wind fields are similar in both cases, providing a favorable environment for the initial development of TCs. In this case, we believe the flow is the dominant factor to TC rather than geopotential height. Note that we only discuss the dynamics here. Other properties of the flow, namely temperature and moisture, need investigation to identify other differences.

In cluster 2, the mature, intense, unstable storms exist in a typical monsoon season field. The 850 hPa level is characterized by a strong WNPSH and a newly formed low-pressure center over the Philippines Sea. The two flows caused by the two systems create a convergence zone where TC is located. After convergence, they form a northwestward flow that leads the translation of TC towards the Asian continent. On 500 hPa, the strong WNPSH is the prominent feature. Adjacent to the WNPSH on the southwest, the TC is led to the northwest by the only counterclockwise circulation flow. In such a situation, the TCs have undergone initial enhancement and shifted into the mature stage, with generally moderate intensity. The TCs will make their next moves: SI, SW, RI, and RW. And the uncertainty is so high, as shown in Fig. 9, that it makes it the most challenging part of TC intensity forecasting. To figure out the reasons causing such variability and factors determining the evolution of TCs, we will provide a case analysis for this cluster and cover it in the next part of this paper.

Cluster 5 represents cases where the TCs reach their peak intensity turning into slow or rapid weakening storms. The monsoon gyre is strong, and along with the withdrawal of WNPSH,

this pattern reduces the easterly flow component on the lower level. The VWS in this cluster has increased from the overall low-shear condition observed in cluster 2. Under the high shear condition caused by reversed-direction airflow between the lower and upper levels, it is plausible that the TCs are tilted and ventilated, and the TC vortex is weakened.

Clusters 6 to 9 capture the dissipation of TCs throughout the year when they reach a relatively high latitude. Under the effect of enormous VWS, the TCs diminishes quickly.

The above discussion is partly attributed to the transitional hypothesis. To validate the transition hypothesis, we will examine the transition of storms from one cluster to another in the subsequent chapter.

CHAPTER 6: TRANSITION ANALYSIS

As mentioned in the last chapter, some clusters are hypothesized to have a sequence relationship. In this chapter, we will verify this relationship by transition analysis.

6.1 Location of TC centroids

Before the analysis, we will examine the location and intensity of each TC as background information. As mentioned in Chapter 2, the TC samples are recorded in a 6-hourly interval from the IBTrACS dataset, and each TC is represented by multiple samples based on its lifetime. Fig. 14 shows the ensemble samples accounted for in this research. Collectively, each cluster has a tremendous geographical distribution of TCs. The shade of color can easily distinguish the intensity. Additionally, some continuous scattered points can be discriminated as the same TC at different times.

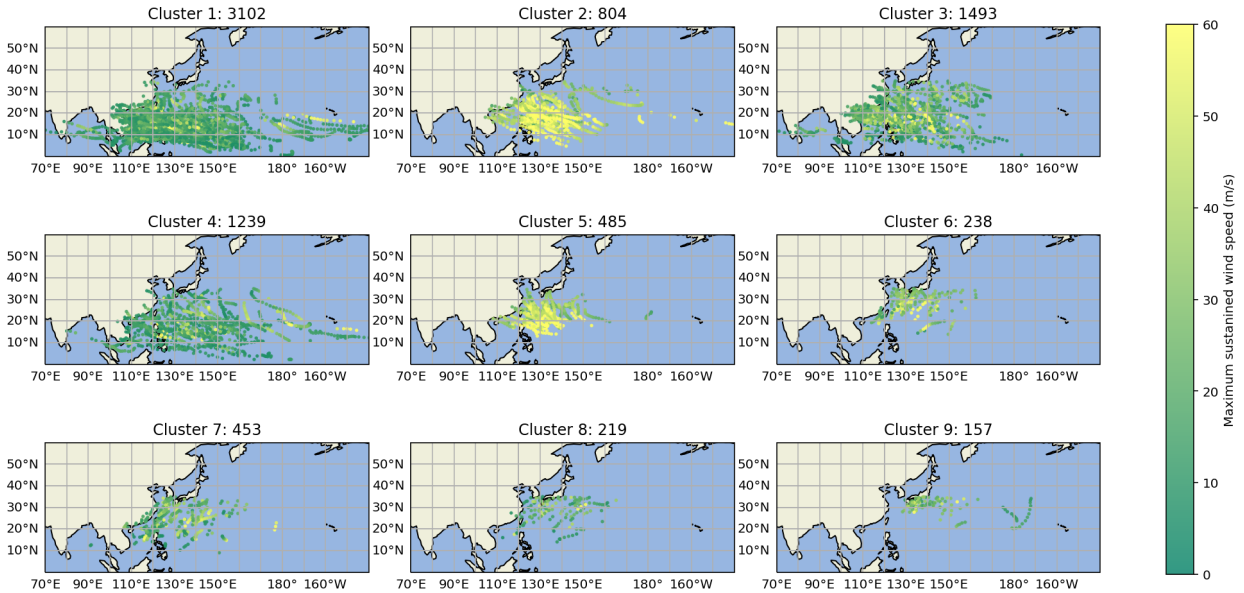

FIG. 14. Centroids of storms (scatters). The intensity is denoted in colors.

6.2 Transitional types and location

In Chapter 2, we have explained that each sample trained by SOMs is assigned to a cluster labeled by cluster index. With the aid of the cluster index, we can find the transition among clusters, defined and derived by the shifts in clustering of the same TC in two consecutive samples at 6-hour intervals. The transition can happen inside the same cluster (internal transition) or between two different clusters (external transition). Discussion of both internal and external transitions will be conducted. Essentially, the analysis of transitions reveals the development of TC through the evolution between clusters.

Fig. 15 shows the transition location and type presented in the target cluster for TC transition. Internal transitions are excluded. For example, cluster 1 has four transition types denoted in red, blue, green, and purple scatters, standing for the transition from cluster 1 to cluster 2, 3, 4, and 7, respectively. These four types happen and are the only ones to happen from cluster 1. Generally, each cluster is associated with 2 to 6 transition types, some of which are more generally seen than the others.

In cluster 1, the transition to cluster 4 is the most common among the four types. It is consistent with our hypothesis in Chapter 5 that cluster 1 and cluster 4 are similar cases. The second most transitions are to cluster 3, hypothesized as the transitional phase.

Cluster 4 displays similarity and dissimilarity to cluster 1. In similarity, it has many transitions to cluster 1, again proving the interaction between clusters 1 and 4. It also contributes to the existence of cluster 2.

Cluster 2 has up to 6 types of transition, except for clusters 8 and 9; The dominant type in this cluster is hard to determine, with all target clusters having a comparable sample size on the

map, corroborating its uncertainty. However, we can safely conclude that clusters 8 and 9 are not directly related to cluster 2 as there are no transitions to these two kinds.

In cluster 5, a significant feature is that no transitions to clusters 1 and 4 are observed. Instead, it will transit to cluster 2 (which is believed to be a similar cluster), cluster 3 (transitional phase cluster), and clusters 6, 7, and 9 (dissipating clusters).

In clusters 6 and 7, multiple transition types are shown. However, most transitions are to what we recognize as late-stage clusters, including clusters 6 to 9. The rest are likely to cluster 3, with so few transitions to clusters 1 and 2 that can be considered outliers.

The target transitions from cluster 8 consist of the remaining late-stage clusters and a small portion of cluster 1. Cluster 9 only witnesses transition to clusters 5 and 8. No transition to cluster 3 is observed in clusters 8 and 9.

Cluster 3 has six transition types. The only transitions that do not happen are (1) from cluster 3 to cluster 9, which may be because cluster 9 is at the end of TC lifetime; (2) from cluster 3 to cluster 4, which is interesting to see. To explain this, if we look at the synoptic maps for these two clusters, we will find that cluster 4 has an immensely strong WNPSH, but cluster 3 has a very weak WNPSH - even weaker than cluster 1. It is impossible for the WNPSH to directly shift from cluster 3 to cluster 4 in 6 hours.

In this figure, the transition types are generally consistent with the previous hypothesis. The stages and transitional relationships are obtained individually, confirming the correlation amongst the clusters. For more quantitative information, the statistics of the transitions are given below.

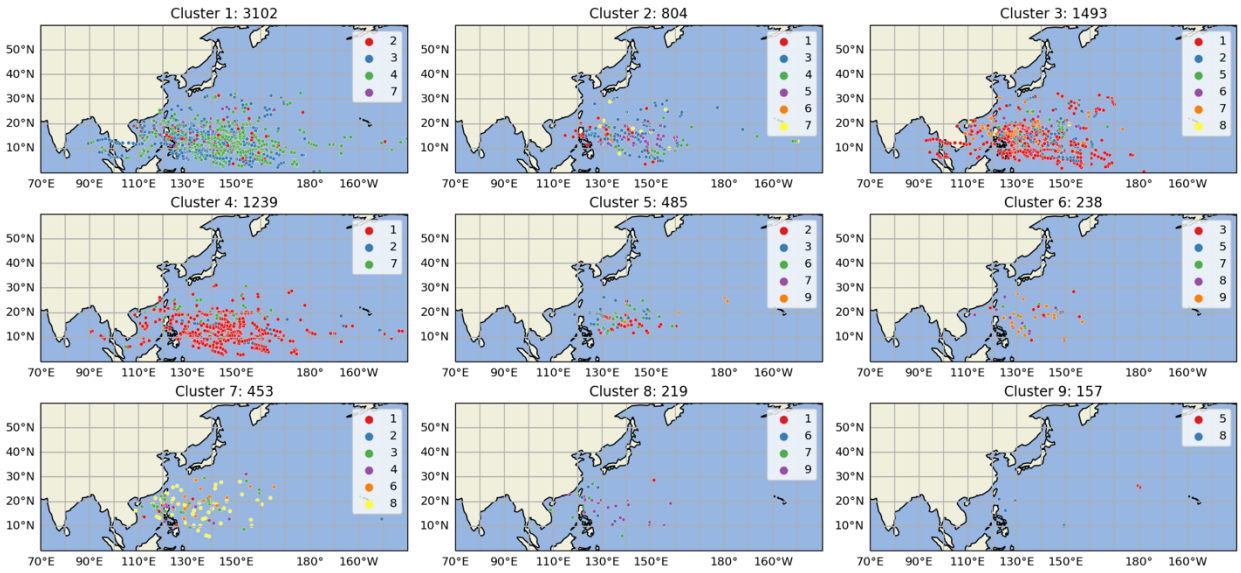

FIG. 15. Transition location (scatters). The transition types are denoted by the colors in the legends.

6.3 Transition charts

The left panel in Fig. 16 shows the transition statistics, including internal transition. The internal transitions are the most frequent transition type for all clusters. The right panel gets rid of internal changes and focuses on the comparison between external changes. From the right panel, it is shown that the transition from cluster 1 to clusters 3 and 4, as well as from clusters 3 and 4 to cluster 1, is the most. Clusters 1 and 2 do not often transit between each other. Again, there is no link between clusters 3 and 4. This reveals that cluster 1 is a transitional phase between clusters 3 and 4. A weak WNPSH in cluster 3 may first intensify to cluster 1, then continue to cluster 4, or a strong WNPSH in cluster 4 may first weaken to cluster 1, then continue to cluster 3. Among other transition types, the transition between clusters 2 and 3 are most seen, suggesting the close transitional relationship between them. Cluster 3 is the most important source and sink for clusters 2 and 5 since it has the most significant ratio into and out of them. The assumed late-stage clusters do not have many transitions.

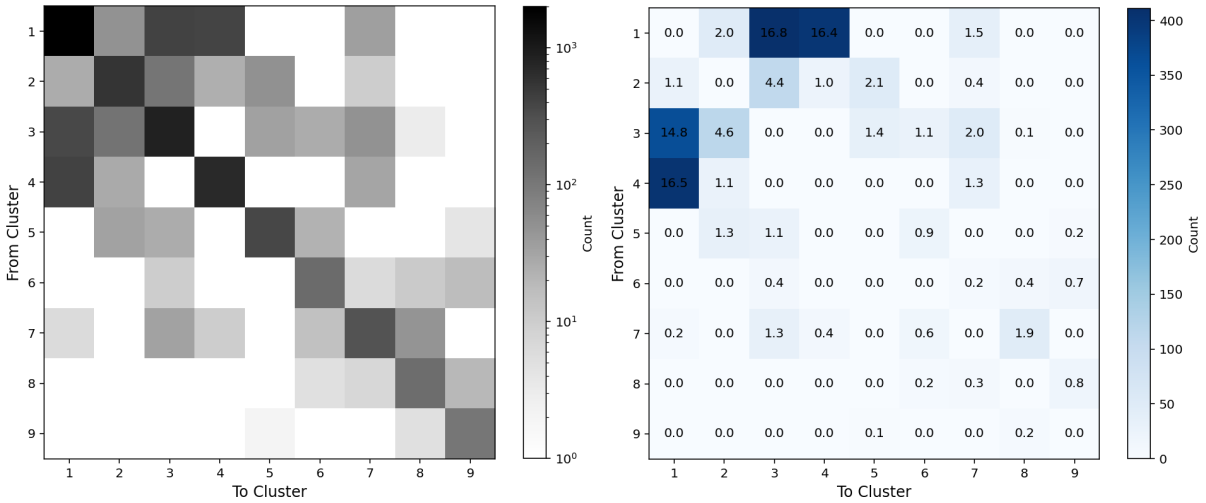

FIG. 16. Transition chart. The original clusters are listed on y-axis, the target clusters are listed on x-axis. The left panel includes internal transitions. The right panel sets all internal transitions equal to 0; the rest of the transition types are divided by the total number of external transitions, denoted in the numbers in the boxes.

6.4 Summary

In summary, there are evident transitional types and rules between clusters, which are similar to and different from the stage distribution we discussed in Chapter 4.2. In Chapter 4.2, we found that clusters are associated with different time periods in TC lifetime, but some of the time periods overlap. In this Chapter, we directly derived that Cluster 1 and 4 are likely the first clusters in TC lifetime; clusters 1 and 3 are related, but clusters 3 and 4 do not have a direct link; cluster 3 is a crucial transitional stage, especially for cluster 2 and 5; cluster 6 to 9 have more inward transitions than outward transitions, confirming that they are sinks.

CHAPTER 7: CASE ANALYSIS: RI/RW

7.1 RI/RW: 850 hPa

In Chapter 4, cluster 2 shows significant variance with high RI and RW rates. Usually, only the samples with similar GPH 500 hPa are assigned to the same cluster. Therefore, it is appealing to see what makes the enormous variability. Fig.17 shows the 850 hPa environment for RI and RW, respectively. As shown by the upper panels, significant differences in TC average location are displayed. RI storms are farther away from the landmass, and the RW is closer to landmass, namely Taiwan and the Philippines. In RI cases, TC has southwesterly flow to the south and easterly flow on the north, where the easterly flow caused by WNPSH is more robust. The two flows converge at the TC and provide environmental vorticity, promoting the rapid intensification of TCs. In RW cases, the WNPSH is weaker, and the southwest monsoon flow is more vigorous. The TC is in the unified south-southeasterly flow formed after the convergence of the two streams. No vorticity is here to contribute to the intensification. The steering flow leading the northward translation of TCs may also be a reason for TC weakening. From the bottom panels, we also find that the northwest outflow differs between the two scenarios: RI has more substantial outflow on the northwest, whereas RW has a weaker outflow. The 1500 hPa isoypse from RI extends from north of TC parallelly to Taiwan and China along 21 degrees latitude, while it extends northwestward and retreats to the east.

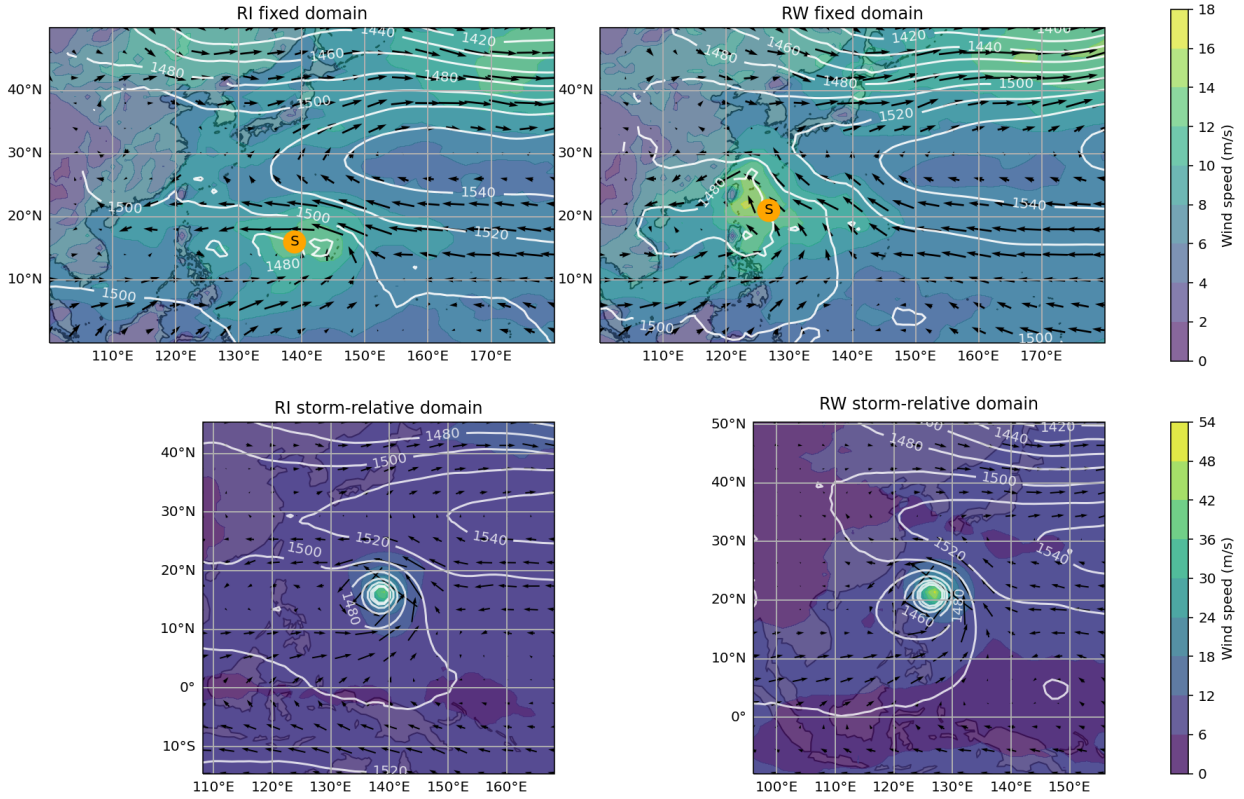

FIG. 17. Geopotential height (contour, hPa) and wind (shaded and barbs, m/s) fields at 850 hPa. The upper panels are averaged over the fixed domain, average TC location marked in orange circle; the bottom panels are dynamically averaged in the storm-relative orientation. The left panels are the composite mean for RI cases; the right panels are the composite mean for RW cases.

7.2 RI/RW: 200 hPa

At the 200 hPa level, TCs in this cluster receive impacts from SAH of similar intensity. Due to the location difference, the RI is more in the easterly wind, while RW is in the center of the anticyclonic gyre.

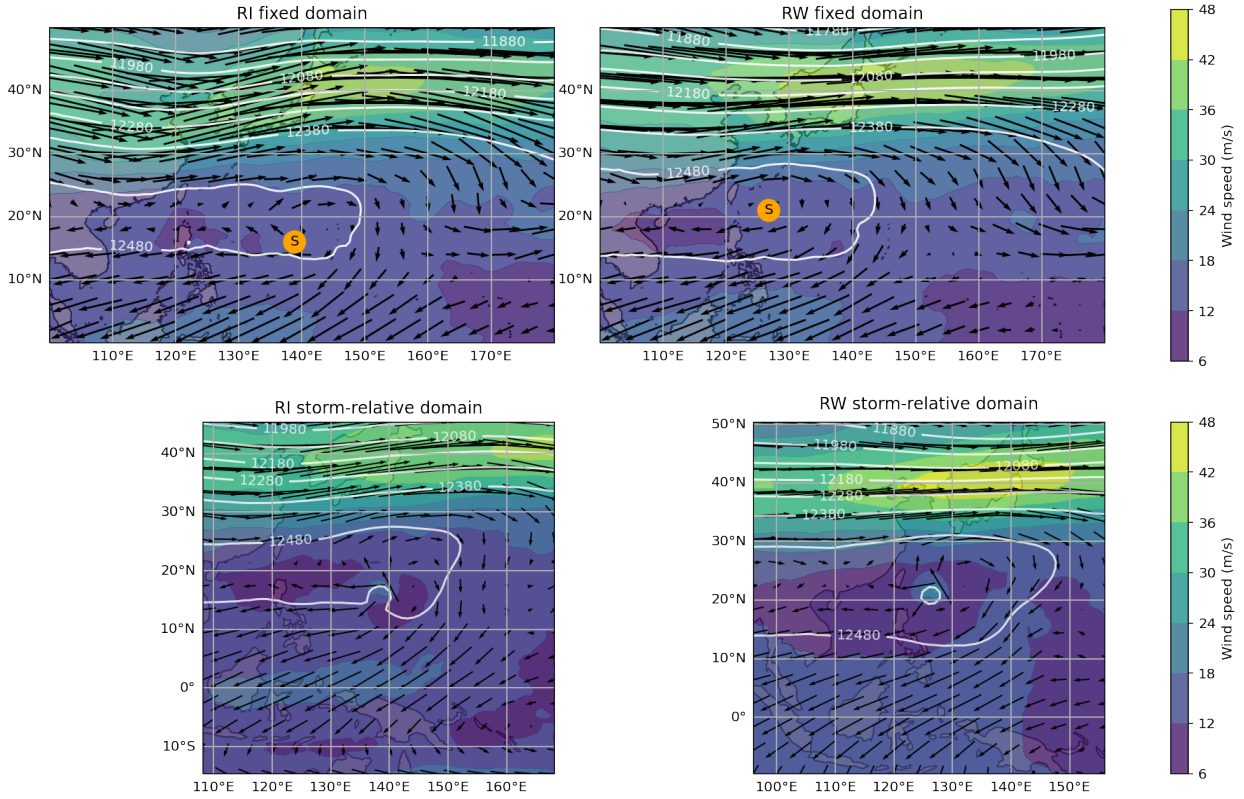

FIG. 18. Geopotential height (contour, hPa) and wind (shaded and barbs, m/s) fields at 200 hPa. The upper panels are averaged over the fixed domain, average TC location marked in orange circle; the bottom panels are dynamically averaged in the storm-relative orientation. The left panels are the composite mean for RI cases; the right panels are the composite mean for RW cases.

7.3 RI/RW: vertical wind shear

Fig. 19 shows the vertical wind shear patterns. Due to the outflow from the TC at upper levels, the wind speed on the upper level is immense, and a high-shear center characterizes the wind shear composite maps for cluster 2 RI/RW. Apart from the center, the wind shear is low. The overall pattern of wind shear is anti-cyclonic, maintaining a symmetric structure.

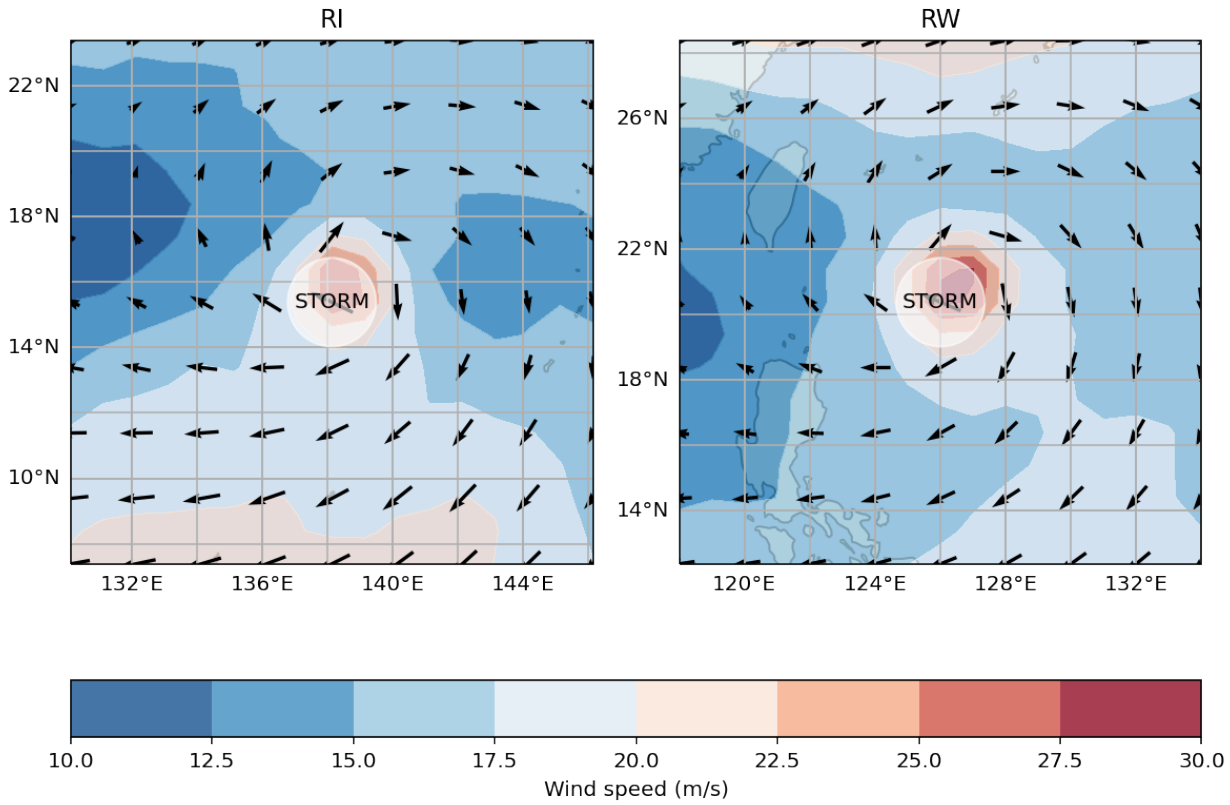

FIG. 19. RI/RW storm-relative total vertical wind shear (shaded and barbs, m/s).

TABLE 2. The average shear statistics

Event	Direction	Magnitude (m/s)
RI	Zonal shear (u shear)	-3.1
	Meridional (v shear)	-2.4
RW	Zonal shear (u shear)	-1.2
	Meridional (v shear)	-2.3

Table 2 shows the horizontal averaged shear statistics for RI and RW. Mutual direction and magnitude of northerly 2.4 m/s are displayed for RI and RW cases in cluster 2 for WNPTCs, which is not consistent with that in the Atlantic Ocean basin; the northerly environmental shear

favors the intensification of TCs, while southerly wind shear is in favor of weakening of TCs (Wadler et al. 2022).

A noticeable gap is seen from the zonal shear that RI has stronger easterly shear. Tuleya and Kurihara (1981) proposed that easterly shear is more favorable for TC genesis, while this hypothesis is also confirmed in the developing or mature stage. However, because the TCs are closer to the equator during RI, the environmental easterly wind is more potent, which may be why the shear is stronger. Since we cannot separate wind shear from other variabilities, no conclusion can be made yet that the easterly wind shear is causing the typhoon to strengthen. However, RI is associated with northerly shear and strong easterly shear.

7.4 Summary

To conclude, two primary differences and one similarity between RI and RW are proposed. The most significant difference is the location. The closer TCs are to landmass, the more likely they will rapidly weaken, and vice versa. The low-level environmental vorticity has an important influence on the intensity change of TCs. Positive environmental vorticity promotes intensification, while zero or negative vorticity contributes to the weakening or rapid weakening of TCs.

Although there are some differences, RI and RW cases are both in cluster 2, which means they share a similar GPH 500 hPa pattern. They both represent intense TCs in the mature stage. The tremendous variability indicates that there may be other factors affecting RI and RW events of TCs in addition to those investigated herein, including thermodynamic (moisture) factors.

CHAPTER 8: CONCLUSIONS

In this thesis, we used SOM to objectively identify and discriminate the GPH 500 hPa patterns in the TC environment. The GPH 500 hPa patterns being an indicator of TC state, different patterns are successfully captured and clustered based on the key features. The relationships with TC activities, e.g., time, stages, intensity, and intensity changes, are investigated, and the composites of large-scale background are explored. Evident correlations between TC activities and synoptic configurations are found and established.

In the earlier stages of the TC lifetime, the TCs are affected by weak southeasterly flow in the lower levels, where slow intensification is most commonly seen. There are two possible patterns in the middle and upper levels: a strong WNPSH with a strong SAH; or a weak WNPSH with a weak SAH. In the former scenario, the TC is inside the WNPSH (5880 m isohypse), enclosing a wide area on the 500 hPa layer and the east edge of SAH (200 hPa). In the latter scenario, the TC is southwest of the weak WNPSH and east of the weak SAH. They are both affected by the WNPSH-caused easterly flow solely on the lower and middle level and northerly flow on the upper level. In wind shear patterns, they are both characterized by a low overall shear in the TC environment, in favor of the TC genesis and development.

In typhoon seasons, two typical clusters of TCs are present in their middle stages, representing the intense storms in these seasons. One of them reflects the middle stage, whose intensity change is volatile. Intense storms usually accompany a strong WNPSH, and the TCs are on its southwest edge, influenced by strong easterly steering flow. On the upper level, a strong SAH is necessary to surround the TC so that the flow is static. Although the environmental

vertical wind shear is small, the TC generates strong anti-cyclonic circulation on the upper level around the center, forming a high shear region.

Nonetheless, the environmental vertical wind shear is higher than in earlier stages due to the TC vortex. Seemingly the high shear does not necessarily prevent the rapid intensification of storms, but we did not separate the environmental shear from the shear caused by the TC itself. More research must be done to investigate the ventilation, environmental effects, and inner processes. The second cluster is representative of the middle to late stages. Evolved from the above cluster, it is more likely to decay rapidly, for it is involved in the strong monsoon gyre. The WNPSH retreats eastward, and the southwesterly monsoon flow forming the gyre is more dominant in modifying the storm. Such configurations also yield increased vertical wind shear, which drives the weakening of TCs.

The late stages are usually associated with TCs moving northward to higher latitudes. When they approach or enter the westerlies, the vast vertical wind shear forms vital ventilation that destroys the TC structure and fosters dissipation.

The analysis of RI/RW in the same cluster proposes a fundamental difference in the zonal component of airflow. RI has a larger easterly shear, while RW has a lower easterly shear. The shear is assumed to relate to the background state, such as moisture, temperature, etc. Those thermodynamic variables are not included in this work but should be a part of future work.

The transitional relationships are discussed in this work, where certain types show relevancy while others show no connection. This is indicative of the development process of TCs, which could benefit a new statistical prediction scheme using SOMs as an objective classifier.

Future work includes a more comprehensive analysis of the thermodynamics fields and separating the storm-created wind fields from environmental factors. Tropical cyclone models of TC evolution could validate the conclusions obtained in this research.

REFERENCES

@misc{vettigliminisom,
  title={MiniSom: minimalistic and NumPy-based implementation of the Self Organizing Map},
  author={Giuseppe Vettigli},
  year={2018},
  url={https://github.com/JustGlowing/minisom/},
}

Aberson, S. D., 2002: Two years of operational hurricane synoptic surveillance. Wea. Forecasting, 17, 1101-1110

Aberson, S. D., 2003: Targeted observations to improve operational tropical cyclone track forecast guidance. Mon. Wea. Rev., 131, 1613-1628

Cangialosi, J. P., & Franklin, J. L. (2012). National Hurricane Center forecast verification report. National Hurricane Center (NHC), 79.

Chang, LC., Chang, FJ., Yang, SN. et al. Self-organizing maps of typhoon tracks allow for flood forecasts up to two days in advance. Nat Commun 11, 1983 (2020). https://doi.org/10.1038/s41467-020-15734-7

Chen, B., Kuo, Y., & Davis, C. A. (2021). Examination of the combined effect of deep-layer vertical shear direction and lower-tropospheric mean flow on tropical cyclone intensity and size based on the ERA5 reanalysis. Monthly Weather Review, 149(12), 4057–4076. https://doi.org/10.1175/mwr-d-21-0120.1

Chen, H., & Zhang, D. (2013). On the Rapid Intensification of Hurricane Wilma (2005). Part II: Convective Bursts and the Upper-Level Warm Core, Journal of the Atmospheric Sciences, 70(1), 146-162. Retrieved Apr 25, 2022, from https://journals.ametsoc.org/view/journals/atsc/70/1/jas-d-12-062.1.xml

DeMaria, M. (1996). The effect of vertical shear on tropical cyclone intensity change. Journal of Atmospheric Sciences, 53(14), 2076-2088.

DeMaria, M., Sampson, C. R., Knaff, J. A., & Musgrave, K. D. (2014). Is tropical cyclone intensity guidance improving?. Bulletin of the American Meteorological Society, 95(3), 387-398.

Emanuel, K. A., 2000: Thermodynamic control of hurricane intensity. Nature, 401, 665-669

Feng, X., & Shu, S. (2018). How do weak tropical cyclones produce heavy rainfall when making landfall over China. Journal of Geophysical Research: Atmospheres, 123, 11,830– 11,848. https://doi.org/10.1029/2018JD029228

Finocchio, P. M., & Rios-Berrios, R. (2021). The intensity- and size-dependent response of tropical cyclones to increasing vertical wind shear. Journal of the Atmospheric Sciences. https://doi.org/10.1175/jas-d-21-0126.1

Frank, W. M., & Ritchie, E. A. (1999). Effects of Environmental Flow upon Tropical Cyclone Structure, Monthly Weather Review, 127(9), 2044-2061. Retrieved Apr 25, 2022, from https://journals.ametsoc.org/view/journals/mwre/127/9/1520-0493_1999_127_2044_eoefut_2.0.co_2.xml

Franklin, J. L., Black, M. L., & Valde, K. (2003). GPS Dropwindsonde Wind Profiles in Hurricanes and Their Operational Implications, Weather and Forecasting, 18(1), 32-44. Retrieved Apr 25, 2022, from https://journals.ametsoc.org/view/journals/wefo/18/1/1520-0434_2003_018_0032_gdwpih_2_0_co_2.xml

Gray, W. M. (1968). Global view of the origin of tropical disturbances and storms. Monthly Weather Review, 96(10), 669-700.

Greg, H. J., & Robert, M. T. (n.d.). On the dynamics of Tropical Cyclone Structural Changes. Retrieved April 25, 2022, from http://www.atmos.albany.edu/daes/atmclasses/atm527/Handouts_files/HollandMerrill_1984.pdf

Guo, L., Klingaman, N. P., Vidale, P. L., Turner, A. G., Demory, M. E., & Cobb, A. (2017). Contribution of tropical cyclones to atmospheric moisture transport and rainfall over East Asia. Journal of Climate, 30(10), 3853-3865.

Guo, Y.-R., Y.-H. Kuo, J. Dudhia, D. Parsons, and C. Rocken, 2000: Four-dimensional variational data assimilation of heterogeneous mesoscale observations for a strong convective case. Mon. Wea. Rev., 128, 619-643

Hannachi, A., Straus, D. M., Franzke, C. L. E., Corti, S., and Woollings, T. (2017), Low-frequency nonlinearity and regime behavior in the Northern Hemisphere extratropical atmosphere, Rev. Geophys., 55 , 199– 234, doi:10.1002/2015RG000509.

Harnos, D. S., & Nesbitt, S. W. (2011). Convective structure in rapidly intensifying tropical cyclones as depicted by passive microwave measurements. Geophysical Research Letters, 38(7).

Harnos, D. S., & Nesbitt, S. W. (2016). Varied pathways for simulated tropical cyclone rapid intensification. Part I: Precipitation and environment. Quarterly Journal of the Royal Meteorological Society, 142(697), 1816-1831.

Houze, R. A., Jr., Chen, S. S., Lee, W., Rogers, R. F., Moore, J. A., Stossmeister, G. J., Bell, M. M., Cetrone, J., Zhao, W., & Brodzik, S. R. (2006). The Hurricane Rainband and Intensity Change Experiment: Observations and Modeling of Hurricanes Katrina, Ophelia, and Rita, Bulletin of the American Meteorological Society, 87(11), 1503-1522. Retrieved Apr 26, 2022, from https://journals.ametsoc.org/view/journals/bams/87/11/bams-87-11-1503.xml

https://web.archive.org/web/20201105102044/http://ndrrmc.gov.ph/attachments/article/1329/FINAL_REPORT_re_Effects_of_Typhoon_YOLANDA_HAIYAN_06-09NOV2013.pdf

https://www.aoml.noaa.gov/hrd/tcfaq/E10.html

Hu, P., Huangfu, J., Chen, W. et al. Impacts of early/late South China Sea summer monsoon withdrawal on tropical cyclone genesis over the western North Pacific. Clim Dyn 55, 1507–1520 (2020). https://doi.org/10.1007/s00382-020-05339-7

Hu, P., Huangfu, J., Chen, W., & Huang, R. (2020). Impacts of early/late South China Sea summer monsoon withdrawal on tropical cyclone genesis over the western North Pacific. Climate Dynamics, 55(5), 1507-1520.

Jaye, A. B., Bruyère, C. L., & Done, J. M. (2019). Understanding future changes in tropical cyclogenesis using Self-Organizing Maps. Weather and climate extremes, 26, 100235.

Kaplan, J., & DeMaria, M. (2003). Large-scale characteristics of rapidly intensifying tropical cyclones in the North Atlantic basin. Weather and forecasting, 18(6), 1093-1108.

Kim, H., & Seo, K. (2016). Cluster Analysis of Tropical Cyclone Tracks over the Western North Pacific Using a Self-Organizing Map, Journal of Climate, 29(10), 3731-3751. Retrieved Apr 25, 2022, from https://journals.ametsoc.org/view/journals/clim/29/10/jcli-d-15-0380.1.xml

Knaff, J. A., Sampson, C. R., DeMaria, M., Marchok, T. P., Gross, J. M., & McAdie, C. J. (2007). Statistical tropical cyclone wind radii prediction using climatology and persistence. Weather and Forecasting, 22(4), 781-791.

Kohonen, T. Self-organized formation of topologically correct feature maps. Biol. Cybern. 43, 59–69 (1982). https://doi.org/10.1007/BF00337288

Komaromi, W. A., & Doyle, J. D. (2017). Tropical Cyclone Outflow and Warm Core Structure as Revealed by HS3 Dropsonde Data, Monthly Weather Review, 145(4), 1339-1359. Retrieved Apr 25, 2022, from https://journals.ametsoc.org/view/journals/mwre/145/4/mwr-d-16-0172.1.xml

Kurihara, Y., Tuleya, R. E., & Bender, M. A. (1998). The GFDL hurricane prediction system and its performance in the 1995 hurricane season. Monthly weather review, 126(5), 1306-1322.

Kurihara. Y, M. A. Bender, R. E. Tuleya, and R. J. Ross, 1998: The GFDL hurricane prediction system and its performance in the 1995 hurricane season. Mon. Wea. Rev., 126, 1306-1322

Lander, M. A. (1994). Description of a Monsoon Gyre and Its Effects on the Tropical Cyclones in the Western North Pacific during August 1991, Weather and Forecasting, 9(4), 640-654. Retrieved Apr 25, 2022, from https://journals.ametsoc.org/view/journals/wefo/9/4/1520-0434_1994_009_0640_doamga_2_0_co_2.xml

Lei Yang, Xi Luo, Sheng Chen, Xiao-Li Zhou, Wei-Qiang Wang, Dong-Xiao Wang, Characteristics of rapidly intensifying tropical cyclones in the South China Sea, 1980–2016, Advances in Climate Change Research, 2022, ISSN 1674-9278, https://doi.org/10.1016/j.accre.2022.04.004.

Ling, Z., Wang, G., & Wang, C. (2015). Out-of-phase relationship between tropical cyclones generated locally in the South China Sea and non-locally from the Northwest Pacific Ocean. Climate Dynamics, 45(3), 1129-1136.

Mcld. (2010, May 19). Somtrain. https://commons.wikimedia.org/wiki/File:Somtraining.svg

Newton, C. W. (1950). STRUCTURE AND MECHANISM OF THE PREFRONTAL SQUALL LINE, Journal of Atmospheric Sciences, 7(3), 210-222. Retrieved Apr 25, 2022, from https://journals.ametsoc.org/view/journals/atsc/7/3/1520-0469_1950_007_0210_samotp_2_0_co_2.xml

Pu, Z.-X., and S. A. Braun, 2001: Evaluation of bogus vortex techniques with four-dimensional variational data assimilation. Mon. Wea. Rev., 129, 2023-2039

Shu, S., Ming, J., & Chi, P. (2012). Large-Scale Characteristics and Probability of Rapidly Intensifying Tropical Cyclones in the Western North Pacific Basin, Weather and Forecasting, 27(2), 411-423. Retrieved Apr 25, 2022, from https://journals.ametsoc.org/view/journals/wefo/27/2/waf-d-11-00042_1.xml

Shu, S., Zhang, F., & Ming, J. (2013, April 1). The Impact of the Western North Pacific Subtropical High (WNPSH) on Tropical Cyclone Intensity. Retrieved April 25, 2022, from https://www.researchgate.net/publication/258774083_The_Impact_of_the_Western_North_Pacific_Subtropical_High_WNPSH_on_Tropical_Cyclone_Intensity

Shu, S., Zhang, F., Ming, J., & Wang, Y. (2014). Environmental influences on the intensity changes of ... Retrieved April 25, 2022, from https://www.researchgate.net/profile/Shoujuan-Shu-2/publication/260830144_Environmental_influences_on_the_intensity_changes_of_tropical_cyclones_over_the_Western_North_Pacific/links/56e9654308ae47bc651c7010/Environmental-influences-on-the-intensity-changes-of-tropical-cyclones-over-the-Western-North-Pacific.pdf

SuperDataScience Team. (2018, September 28). The Ultimate Guide to Self Organizing Maps (SOM's). https://www.superdatascience.com/blogs/the-ultimate-guide-to-self-organizing-maps-soms

Tallapragada, V., Kieu, C., Kwon, Y., Trahan, S., Liu, Q., Zhang, Z., & Kwon, I. H. (2014). Evaluation of storm structure from the operational HWRF during 2012 implementation. Monthly Weather Review, 142(11), 4308-4325.

Tuleya, R. E., & Kurihara, Y. (1981). A Numerical Study on the Effects of Environmental Flow on Tropical Storm Genesis, Monthly Weather Review, 109(12), 2487-2506. Retrieved Apr 25, 2022, from https://journals.ametsoc.org/view/journals/mwre/109/12/1520-0493_1981_109_2487_ansote_2_0_co_2.xml

Tuleya, R. E., & Kurihara, Y. (1981). A numerical study on the effects of environmental flow on tropical storm genesis. Monthly Weather Review, 109(12), 2487-2506.

Wadler, J. B., Cione, J. J., Zhang, J. A., Kalina, E. A., & Kaplan, J. (2022). The Effects of Environmental Wind Shear Direction on Tropical Cyclone Boundary Layer Thermodynamics and Intensity Change from Multiple Observational Datasets, Monthly Weather Review, 150(1), 115-134. Retrieved Apr 25, 2022, from https://journals.ametsoc.org/view/journals/mwre/150/1/MWR-D-21-0022.1.xml

Wang, B., R. L. Elsberry, Y. Wang, and L. Wu, 1998: Dynamics in tropical cyclone motion: A review. Chinese J Atmos Sci, 22, 535-547.

Wang, C., Wang, B. Impacts of the South Asian high on tropical cyclone genesis in the South China Sea. Clim Dyn 56, 2279–2288 (2021). https://doi.org/10.1007/s00382-020-05586-8

Wang, Y., Wu, CC. Current understanding of tropical cyclone structure and intensity changes – a review. Meteorol Atmos Phys 87, 257–278 (2004). https://doi.org/10.1007/s00703-003-0055-6

Wong, M. L., & Chan, J. C. (2004). Tropical cyclone intensity in vertical wind shear. Journal of the atmospheric sciences, 61(15), 1859-1876.

Wu, C.-C., K.-H. Chou, P.-H. Lin, S. Aberson, et al. 2007: The impact of dropwindsonde data on typhoon track forecasts in DOTSTAR. Wea. Forecasting, accepted for publication

Wu, C.-C., P.-H. Lin, K.-H. Chou, W.-P. Huang, and J.-H. Chen, 2006: The impact of the dropwindsonde data and the targeted observation in DOTSTAR. Workshop on Weather Research and Forecasting (WRF) Mode and Data Assimilation, Taipei, Taiwan

Wu, L., Wang, B., and Geng, S. (2005), Growing typhoon influence on east Asia, Geophys. Res. Lett., 32, L18703, doi:10.1029/2005GL022937.

Wu, Q., Wang, X. & Tao, L. Interannual and interdecadal impact of Western North Pacific Subtropical High on tropical cyclone activity. Clim Dyn 54, 2237–2248 (2020). https://doi.org/10.1007/s00382-019-05110-7

Zhang, W., Zhang, Y., Zheng, D., Wang, F., & Xu, L. (2015). Relationship between lightning activity and tropical cyclone intensity over the northwest Pacific. Journal of Geophysical Research: Atmospheres, 120(9), 4072-4089.